Johannes Kepler University Linz Faculty of Engineering and natural Sciences

University of South Bohemia in České Budějovice
Faculty of Science

Characterization of TbPH1, a kinetoplastid-specific pleckstrin homology domain containing kinesin-like protein

MASTER THESIS

Sabine Kaltenbrunner

Cross-Border joint Master's Program
Biological Chemistry

Supervisor: Hassan Hashimi, Mag. Ph.D.

Institute of Parasitology, Biology Centre, Academy of Sciences of Czech Republic
and
Faculty of Science, University of South Bohemia

České Budějovice, 2017

Kaltenbrunner S., 2017. Characterization of TbPH1, a kinetoplastid-specific pleckstrin homology domain containing kinesin-like protein. MSc. thesis in English, 63p, Faculty of Science, University of South Bohemia, České Budějovice, Czech Republic

Annotation

The aim of this master thesis was the investigation of the uncharacterized protein TbPH1, by *in silico* studies, determining effects of its knock-down, studying the effects of a knock-down on the cell cycle, examining its cellular localization, and finding out about possible complexes and interaction-partners.

Annotation

Das Ziel dieser Arbeit war die Untersuchung des uncharakterisierten Proteins TbPH1. Neben in silico Studien sollten auch generelle Knock-down Effekte und dessen Auswirkung auf den Zellzylkus und die zelluläre Lokalisierung bestimmt werden. Weiters sollte auch herausgefunden werden, ob TbPH1 Teil eines Proteinkomplexes ist und mögliche Interaktionspartner sollten bestimmt werden.

Affirmation

I hereby declare that, in accordance with Article 47b of Act No. 111/1998 in the valid wording, I agree with the publication of my bachelor thesis, in full to be kept in the Faculty of Science archive, in electronic form in publicly accessible part of STAG database operated by the University of South Bohemia in České Budějovice accessible through its web pages.

Further, I agree to the electronic publication of the comments of my supervisor and thesis opponents and the record of the proceedings and results of the thesis defence in accordance with aforementioned Act. No. 111/1998. I also agree to the comparison of the text of my thesis with the Thesis.cz thesis database operated by the National Registry of University and a plagiarism detection system.

České Budějovice, 18.04.2017

_____

Sabine Kaltenbrunner

Sworn Declaration

I hereby declare under oath that the submitted Master's degree thesis has been written solely by me without any third-party assistance, information other than provided sources or aids have not been used and those used have been fully documented. Sources for literal, paraphrased and cited quotes have been accurately credited. The submitted document here present is identical to the electronically submitted text document.

České Budějovice, 18.04.2017

_____

Sabine Kaltenbrunner

Acknowledgement

I am grateful to have had the opportunity to work in the laboratory of Prof. Julius Lukeš. It was a fulfilling and exciting experience. I am especially thankful for the guidance of my supervisor Hassan Hashimi, Mag. Ph.D. as he provided valuable advice in times when needed but let me the freedom to explore by myself in other times. It was him that never gave up on me in even the toughest times.

I also would like to thank my students Hannah Bruce and Quentin Oliveres. In my experience, teaching is never a one-way street and I learned at least as much from them as they did from me.

Special thanks also to all the other people in the laboratory who are one the reasons why working in this laboratory was such a nice experience by creating a good working environment.

Abbreviations

AA	Amino Acid
ATP	adenosin triphosphate
BSA	Bovine Serum Albumin
BSF	Bloodstream Form
DAPI	4',6-DiAmidino-2-PhenylIndole
DMSO	DiMethyl SulfOxide
DNA	DeoxyriboNucleic Acid
FACS	Fluorescence Assisted Cell Sorting
FAZ	Flagellum Attachment Zone
FT	Flow Through
GTP	Guanosine Triphosphate
HAT	Human African Trypanosomiasis
Hyg	Hygromycin
IFA	ImmunoFluorescent Assay
IP	ImmunoPrecipitation
MAPs	Microtubule-Associated Proteins
MeOH	Methanol
MTS	MicroTubule-Sieving
NC	Negative Control
P	Pellet
PBS	Phosphate Buffered Saline
PCF	Procyclic Form
PCR	Polymerase Chain Reaction
PFR	ParaFlagellar Rod
PH-domain	Pleckstrin Homology-domain
pPOT	plasmid PCR Only Tagging
RNAi	RNA interference
SDS	Sodium Dodecyl Sulphate
SMART	Simple Modular Architecture Research Tool
SmOxP	Singlemarker Oxford Procyclic
SN	Supernatant
TEA	TriEthanolAmine
TX	Triton-X 100
UTR	UnTranslated Region
VSGs	Variant Surface Glycoproteins
WCL	Whole Cell Lysate

Table of Contents

1. INTRODUCTION

1.1 The model organism *Trypanosoma brucei*

Trypanosoma brucei is a flagellated protozoan parasite that belong to the class Kinetoplastida. They are early-branching in the phylogenetic tree [13] Subspecies of the parasite are the causative agents of diseases like Human African Trypanosomiasis (HAT), or nagana in ruminant animals [1].

T. brucei are heteroxeneous parasites with mammals as its intermediate host and the tse-tse fly (*Glossinidae Glossina*) as the vector. Because of its digenetic life cycle, the parasite is exposed to very different environments to which it has to adapt, leading to profound changes in its surface coating, morphology, and energy metabolism [2, 3, 4].

During its complicated life cycle (Figure 1), *T. brucei* differentiates into its various forms: Firstly, the tse-tse fly takes a bloodmeal from an infected intermediate host and takes up the short stumpy form of *T. brucei* [6]. The parasite then differentiates into procyclic (PCF) trypanosomes, which proliferates in the midgut of the insect. They subsequently migrate through the peritrophic matrix, to the proventriculus, through the mouthparts to the salivary glands, where they differentiate into epimastigotes [7]. In the salivary glands, they then undergo preparation to infect another mammalian host as the non-proliferating metacyclic form of the parasite. The infection starts by the blood meal of the insect, taking up the metacyclic *T. brucei*. Inside the mammalian host, *T. brucei* proliferates as the long slender form in the bloodstream (BSF *T. brucei*). It then differentiates into the non-proliferating short stumpy form, which is ready for being taken-up by the next fly vector. [8] In the laboratory, two proliferating life stages are regularly worked with: the

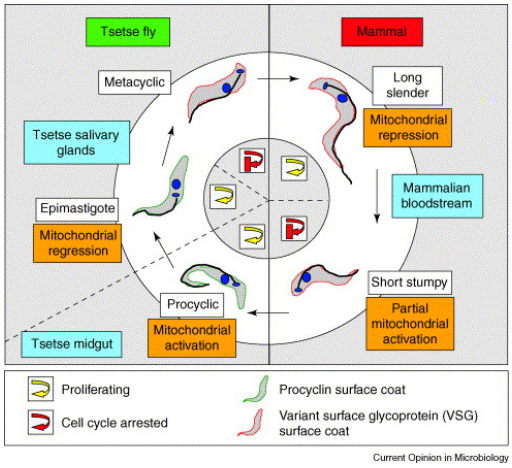

Figure 1: Life cycle of *T. brucei*; Taken from [21]

long slender bloodstream form and the procyclic form. Both have fast generation times and can be easily cultured *in vitro* [9].

As a model organism, *T. brucei* is well established, with a fully sequenced genome available [10]. In addition, there are many tools at hand for genetic manipulation of the parasite, such as endogenous tagging or generating knock-out genes through homologous recombination. The possibility of using tetracycline-inducible RNA interference (RNAi) or ectopic overexpression is another advantage.

However, a recent study by Moullan and coauthors [11] has shown that tetracycline itself has an impact on diverse eukaryotic model systems, raising concerns about the use of tetracyclines confounding experimental outcomes. In the study, it was shown that tetracyclines have an effect on mitochondrial translation, leading to a mitonuclear protein imbalance and ultimately impacting the physiology of several model organisms [11]. However, we were able to show that this is not the case for *T. brucei*, due to its highly divergent nature of its mitochondrial ribosome [12, see Appendix].

As trypanosomes are branching-off early in the phylogenetic tree, they are highly evolutionarily diverged from other eukaryotes [13]. As such, also their cell structure is different from other eukaryotes: they have simple cell architecture with a single or only a few copies of some of their organelles (Figure 2).

1.2 Cell Structure of *T. brucei*

The shape of *T. brucei* is maintained by a dense array of subpellicular microtubules beneath the plasma membrane. Those microtubules are highly cross-linked by microtubule-associated proteins (MAPs) [14,15,16].

On the surface, bloodstream form *T. brucei* expresses one of a multitude of possible variant surface proteins (VSGs) that can be randomly switched in order to evade the immune response of the mammalian host [17]. The procyclic form of the parasite does not express VSGs but a different set of invariant glycoproteins: the procyclins [18].

At the posterior end of the parasite, a single flagellum exits the cell from the flagellar pocket, which is the only site of endo- and exocytosis in *T. brucei* [16].

The flagellum is connected to the cell body via the flagellum attachment zone (FAZ) [19, 20]. Alongside the mature basal body, from which the flagellum arises, an immature pro-basal body is situated. During the progression of the cell cycle, the pro-basal body starts to mature and the daughter flagellum starts to grow from this structure [21]. In close proximity to the basal bodies are the Golgi bodies. A cell in G1 phase contains in average either one or two Golgi bodies, which are situated beneath the flagellum and are located at the FAZ [22, 23].

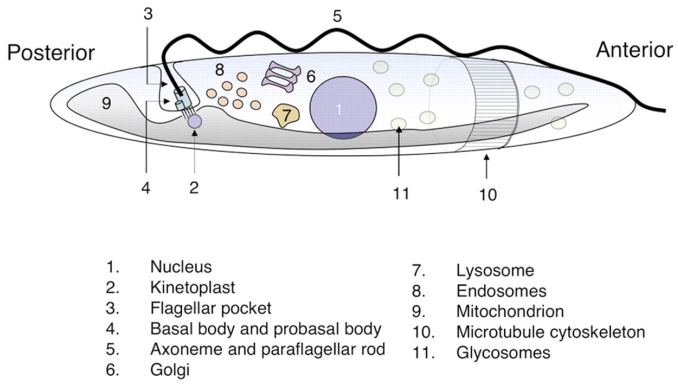

Figure 2.: Basic cell structure of *T. brucei*
Taken from [4]

One peculiar feature about *T. brucei* is their single mitochondrion. It contains a single mitochondrial DNA network termed the kinetoplast, which is associated with the basal body. The mitochondrion changes drastically during the life cycle: in the procyclic stage, the organelle is elaborate and contains cristae, which are lacking in the bloodstream stage. In the bloodstream life cycle stage, *T. brucei* is solely relies on glycolysis for its energy metabolism. For the process of glycolysis, *T. brucei* has specialized multicopy organelles derived from peroxisomes, termed the glycosome that contain enzymes needed for glycolysis [24]. Another multi-copy *T. brucei* organelle are acidocalcisomes, which serve to store calcium [25].

1.3 Cell Cycle of *T. brucei*

In general, the eukaryotic cell cycle consists of two major events: the replication of DNA (S-phase) and mitosis (M-phase). The two phases are separated by two gap phases, called the

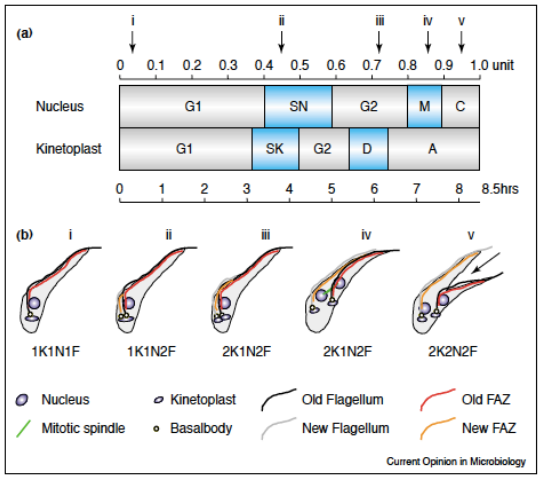

Figure 3.: Cell cycle of *T. brucei*. SN: S-phase, nucleus; SK: S-phase, kinetoplast; D: Division; A: Apportioning phase (basal bodies continue to move apart) K: Kinetoplast; N: Nucleus; Taken from [21]

G1 and G2 phases (Figure 3) The whole process needs to be tightly regulated to proceed in the right order and to occur only once per cell cycle.

In trypanosomes, the cell cycle is slightly more complicated: Firstly, in addition to the nuclear S-phase, the kinetoplast goes through a discrete DNA synthesis phase as well. Secondly, during the cell cycle of *T. brucei*, the many single copy organelles have to be accurately duplicated, segregated and positioned at specific locations. All of this has to happen in a precisely orchestrated and ordered process [26].

The first event to happen in a new cell cycle is the elongation and maturation of the pro-basal body [16]. This step permits the nucleation of a new flagellum. Next, the duplication of the Golgi apparatus happens. During this time, overall cell volume, mitochondrial volume and the number of glycosomes increases [23]. Afterward, the replication of the kinetoplast (S_K-phase) initiates, which happens immediately before the onset of nuclear S_N-phase. The S_K-phase is shorter than the nuclear one and the kinetoplast divides before mitosis starts [27]. The basal bodies then separate during the $G2_N$-phase (the nuclear G2-phase), which is important for the segregation of the kinetoplast [28]. Afterwards, the nucleus goes through mitosis, which is a closed one in trypanosomes, meaning that the nuclear envelope does not break down during the process [29]. Cytokinesis occurs then longitudinally along the cell, with the cleavage furrow starting from the anterior, in between the two flagella, and extends towards the posterior of the cell [16].

During the life cycle of *T. brucei*, proliferating forms are changing into cell cycle arrested stages that are prepared for transmission to the next host. After this transmission, the cell cycle arrest is released and the parasite returns to a proliferate state [30, 31].

1.4 PH-domains

The pleckstrin homology (PH) domain is present two times in a protein named pleckstrin. The name is derived from its function- **P**latelet and **L**eukocyte **C** **K**inase **S**ubstrate [32]. The domain is

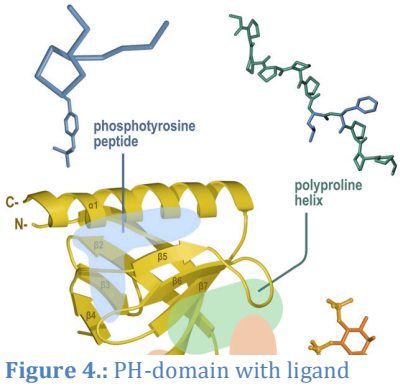

Figure 4.: PH-domain with ligand binding sites . Taken from [35]

usually about 100 amino acids long. At the primary structural level, PH-domains do not share much similarity. However, its three-dimenstional structure is highly conserved (Figure 4) [33, 34]. When elucidating the first structures [35, 36], it was found that the domain has a bent seven-stranded antiparallel β-sheet, which was closed on one side by a C-terminal α-helix [33]. Proteins containing a PH-domain were found to be involved in signaling [38], cytoskeletal organization [39], membrane trafficking [40] and phospholipid processing [41].

1.5 Kinesins

Kinesins are a superfamily of motor proteins that move along microtubule filaments, which is powered by ATP hydrolysis [42]. The motor domain of kinesins, termed the head, is well conserved among the superfamily [43, 44]. It is usually attached to a coiled-coil stalk and tail, the latter of which functions in binding cellular cargo for transportation. The position of the head is not conserved within the protein, being located for instance N-terminally in Kinesin-1, C-terminally in Kinesin-14 and centrally in Kinesin-13 [45]. The catalytic core of the motor domain consists of an eight-stranded beta-sheet with three alpha-helices on each side. There, at the central beta-sheet, it has a nucleotide-binding cleft with a highly conserved P-loop motif (GXXXXGK[TS]). On the opposite side of this beta-sheet is the binding site that associates with the microtubule. This site interacts with tubulin via the structural elements L11-α4-L12-α5. As ATP is hydrolysed, two very conserved domains, called SwitchI with a SSRSH motif and SwitchII with a DLAGXE motif, go through a conformational change. In myosins, whose motor domain is the same as kinesins, SwitchI and II are responsible for closing the nucleotide binding cleft, which enables the motor domain to hydrolyze ATP [46, 47, 48]. As the head is highly conserved within the kinesin superfamily, differences in function, speed and direction of movement are due to parts outside of the catalytic core, such as the stalk or the tail [49].

However, not all kinesins are moving the same amount of steps along microtubules. When Kinesin-1 for instance binds to a microtubule, it hydrolyses more than hundred ATPs, each time making one step forwards, before it detaches again [50, 51, 52]. In contrast, Kinesin-14 binds to a microtubule,

hydrolyses only one ATP and disassociates [53, 54].

Among the cellular functions of kinesins are transportation of cargo from the cell center to the periphery and aiding in mitosis and meiosis. The latter two roles are mediated by either stabilizing or destabilizing microtubules and thus controlling their length [55, 56, 57]. In addition, kinesins that interact with themselves antiparallelly, like Kinesin-5, can bind with their respective heads to two microtubules and slide them in opposite directions during mitosis [58].

The association of kinesins is not exclusively homogenic. Some kinesins can bind to other proteins via their stalk. Often, di- or multimerization into homo- or heteromers has a regulatory effect on motor activity. An example for this regulatory effect is Kar3, which is the Kinesin-14 homolog of budding yeast. Kar3 can dimerize into a homodimer or with two other proteins, Vik1 and Cik1 that have no motor-domain themselves [59, 60]. When associating with Cik1, Kar3 changes its conformation and is changed into a faster motor [61].

1.5.1 Walker motifs

In 1982, John E. Walker investigated the alpha and beta subunits of the ATP synthase binding complex and compared its sequence to other ATP-requiring enzymes. What he found was a persistent sequence similarity in especially two parts [114] – these parts were then termed the Walker A and the Walker B motif. The motifs can be found in ATP and GTP-using proteins and are involved in binding and hydrolyzing ATP [115]. The Walker A motif is essential for binding the phosphate group of ATP and consists of the conserved amino acid pattern GXXXXGK[TS], with X indicating any amino acid and lysine being the crucial residue for binding the β-phosphate of the nucleotide [115,114].

The amino acid pattern of the Walker B motif is [RK]XXXXGXXXXLhhhhD, with h indicating a hydrophobic amino acid [115, 114]. The aspartic acid of the motif is highly conserved. Hydrogen-bonds with these residues with the threonine and serine of the Walker A motif aid in hydrolysis [116].

Most large bacteriophage terminases do contain a Walker A motif in their N-terminus. However, there are other terminases that lack the classical, conserved sequence but instead have a deviant form of the Walker A motif. The deviation

consists of a missing lysine residue that is critical for phosphate-binding. Instead, those terminases have a lysine residue at the N-terminal end of the Walker A motif, which makes the terminase functional again. [112].

1.6 Homeodomains

The homeodomain is a DNA-binding motif, which is about 60 amino acids long. It was first discovered at the beginning of the 1980s in *Drosophila.* [62, 63]. As structural studies (X-ray crystallography and NMR spectroscopy) revealed, the general structure of the homeodomain consists of three alpha-helices that are connected by a short loop and folded into an overall globular shape. The first two helices on the N-terminus are parallel to each other and the third helix on the C-terminus is positioned perpendicular with respect to the first two helices. The C-terminal alpha-helix is the one that interacts with DNA and is therefore also referred to as the "recognition helix" [64-72].

Besides the classical function of DNA-binding, homeodomains are also found in RNA binding proteins [73] and in protein-protein interactions [74].

1.7 Kinesins in *T. brucei*

In the year 2006, a kinesin phylogeny study by Bill Wickstead and Keith Gull identified 41 putative kinesin sequences in *T. brucei* with 13 kinesin-like proteins that are specific for kinetoplastids [75]. In this study, it was revealed that the parasite is missing entire kinesin families. However, this fact is nothing unusual as no organism contains every known kinesin family. The function of the missing kinesins is likely fulfilled by other kinesins, such as the so-called "orphan" kinesins. Orphan kinesins are highly divergent and therefore not grouped into any of the 14 kinesin families. A surprising finding from this study is that *T. brucei* has five Kinesin-13 members, which is an unusually high number compared to for instance to humans that only have 3 [75]. Members of the Kinesin 13 family are in general involved in microtubule depolymerization [76, 77] and vesicle transport [78]. In *T. Brucei*, a member of this family - TbKIF13-2 - was studied with respect to flagellar length control. It was found that its overexpression lead to a mild increase in flagellar length as compared to

control cells. The deletion of TbKIF13-2 had a slight effect on initial growth of the developing, new flagellum [79]. Another member of the kinesin 13 family – TbKif13-1 – is involved in regulating spindle length during mitosis and is essential in both procyclic and bloodstream form *T. brucei* [80].

Later, in a review about the evolution of kinesins in 2015 [81], it was stated that *T. brucei* lack the Kinesin-Family numbers 5, 6, 10, and 11 and from Kinesin-Family numbers 3, 4, and 14, one kinesin is missing in each. Members of the Kinesin 6 family have found to function in microtubule transport [82] or in cytokinesis [83, 84]. They are completely absent from plant species. The Kinesin 10 family was found to play a role in chromosomal movements in cell division. The first member of Kinesin family 11 was Smy1, which was found not to bind to microbutules most likely due to its having a divergent catalytic core [85]. The members of this family were found to be involved in signal transduction [86] and are probably not motile along microtubules [87]. The Kinesin-5 family is very conserved with KIF11 as the predominant member, which forms homotetramers [88] that facilitate the formation of mitotic spindle [89]. Its absence in mitosis is surprising considering the high conservation of the kinesin. However, it seems that, in contrast to previous bioinformatic studies, the genome of *T. brucei* still contains a homolog of KIF11 [75].

Other studied kinesins in *T. brucei* include TbKIN-A and TbKIN-B, which are two divergent orphan kinesins that assist in spindle assembly and chromosome segregation [91]. TbKIN-C is needed for cytokinesis and maintenance of cell morphology [92] and interacts with TbKIN-D to regulate subpellicular microtubules [93].

2. MATERIALS AND METHODS

2.1 Cultivation of *Trypanosoma brucei*

Procyclic *Trypanosoma brucei* were cultivated in SDM-79 medium containing 10% of fetal bovine serum and 2.5 µg/mL hemin. Cells were grown at 27 °C [94]. The parental cell line used for procyclic *Trypanosoma brucei* was the single marker SmOxP9 cell line [95]. SmoxP9-cells were grown in media containing 1 µg/mL puromycin to sustain the T7 RNA polymerase and tetracycline repressor gene introduced into the TREU927/4 cell line [96]. The *in situ* C-terminally V5-tagged cell-line (TbPH1-V5) was grown in the presence of the additional selective drug hygromycin at a concentration of 50 µg/mL.

Table 5: Cell lines of TbPH1 and corresponding selective drugs.

Cell lines of TbPH1	**Procyclics:** **Selective Drugs [Concentration]**	**Bloodforms:** **Selective Drugs [Concentration]**
C-terminal tag	Puromycin [1 µg/mL] Hygromycin [50 µg/mL]	Blasticidin [5 µg/mL] Hygromycin [5 µg/mL]
N-terminal tag HA	Puromycin [1 µg/mL] Blasticidin [10 µg/mL]	Blasticidin [5 µg/mL]
TbPH1-RNAi	Puromycin [1 µg/mL] Hygromycin [50 µg/mL] Phleomycin [2.5 µg/mL]	Blasticidin [5 µg/mL] Hygromycin [5 µg/mL] Phleomycin [1.25 µg/mL]

The N-terminally HA-tagged cell-line (HA-TbPH1) and TbPH1-RNAi cell-line were grown in the presence of the blastidicidin (10 µg/mL) and phleomycin (2.5 µg/mL), respectively.

Long slender bloodform *Trypanosoma brucei* were cultivated in HMI-9 media, supplemented with 10% fetal bovine serum. The parental cell line used was the 2T1:T7 [97].

For growth-curves of procyclic *Trypanosoma brucei*, the cell density was counted every day with the Z2 cell counter and diluted to 2 x 10^6 cells/mL, with media supplemented with the appropriate selective drugs and 1 µg/mL tetracycline to

induce RNAi. Growth-curves of long slender bloodform *Trypanosoma brucei* were done like procyclics cells but the dilution was done to 2 x 10^5.

2.2 Generation of TbPH1-cell lines

TbPH1 was endogenously tagged on both C- and N-terminus using the **P**CR **O**nly **T**agging approach mediated by the pPOTv4 vector [98]. The technique works by amplifying a tag and a resistance cassette encoded by the pPOT-vector with long oligonucleotides. The primers contain 80 nucleotides of homology. For the N-terminal tagging, the forward primer has homology at the end of the 5' UTR, the reverse primer at the start of the open reading frame. In case of the C-terminal tagging, homology flanks of the primers are chosen from the end of the gene, omitting the stop codon (forward-prime) and to the first 80 nucelotides of the 3' UTR (reverse-primer). The used primers are summed up in table 2. The original pPOTv4 vector was modified by replacing the original eYFP-tag between the HindIII and BamHI sites once with HA and V5 and the resistance marker for C-terminal tagging. This modification resulted in a pPOTv4-V5 vector with G418 and a pPOT-HAv4 vector with hygromycin as resistance marker for C-terminal tagging. The C- and N-terminus of TbPH1 was tagged with V5 and HA, respectively.

Table 6: Primer sequences for N- and C-terminal tagging of TbPH1. Upper case letters correspond to sequence of gene/untranslated region for homologous recombination in *T. brucei*. Lower case letters are annealing to the pPOT-vector for amplification of tag and resistance cassette.

Primer name	Primer sequence (5'- 3')
N-term. HA-TbPH1, FW	AAAACGGGAAAAAGTTAAGAGAACAATCATAGGGCAAT AAAATAAGGCCAGATTTTCGCACAGGTGATAAACAGGA AACAgtataatgcagacctgctgc
N-term. HA-TbPH1, RV	TTATCTACTGACAGAGCTGGGGGAATGCTCAGCGTTGGT AACTTGAGCGAGTGCGCACAGAACACAAGTTTCGCATCC ATactacccgatcctgatcc
C-term. TbPH1-V5, FW	TTTCTTCCGGTCTTGACTTATTCCGCTCAGGGAAGCTTT ATGATTTCTTATGCGAAAAGAGAGTCATACCGCTCCCGT ACggttctggtagtggttcc
C-term. TbPH1-V5, RV	ATAATAAAGAGGAAGGGAAGGTAAAGTTCAGAAACAAA TTCTGTTGGCTCCTGATAACACTCTCATATTTCCTTCAC CGCccaatttgagagacctgtgc

The PCR-product was then directly used for electroporation into PF or BF *T. brucei* with hygromycin or blasticidin as selective drug, respectively.

For the TbPH1-V5-RNAi cell line, a fragment of the gene of TbPH1 was PCR-amplified from genomic DNA of *T. brucei* with the forward primer TATggatccGTTGCGTGATGAGCTTCAAA (lower case BamHI) and the reverse primer ACGaagcttCTCCTCTAGCACCGTTTTGC (lower case HindIII). The gene fragment was then cloned with the mentioned restriction sites into the p2T7-177 vector [90]. The construct was then linearized with the restriction enzyme NotI and electroporated into PCF and BSF *T. brucei* as described in [99].

2.3 Indirect Fluorescence Assay (IFA)

2.3.1 Protocol of Indirect Fluorescence Assay (IFA)

Approximately 2 x 10^6 cells were taken per slide,. In the case of mitochondrial staining, MitoTracker® Red CMXRos (Invitrogen) dissolved in DMSO was added directly to the media to a final concentration of 50 nM (PCF) or 10 nM (BSF), and incubated for 30 minutes at 27 °C or 37 °C, respectively.

The cells were then spun down at 1100 x *g* for 3 minutes, supernatant was aspirated and the cells were washed once in 1 mL of PBS. They were then resuspended in 200 µL PBS and fixed by addition of 300 µL of 4% paraformaldehyde in PBS for about 30 minutes. Cells were spun down, washed once in 1 mL of PBS, resuspended in 100 µL PBS and applied to Superfrost plus® slides (Thermo Scientific).

The slides were then washed twice more with 0.1M glycine in PBS to inactivate any residual formaldehyde. The slides were incubated overnight in methanol at -20 °C to permeabilize the cells. The next day, the slides were rehydrated by washing them two times in PBS. The cells were blocked in 1% BSA in PBS for one hour in a humid chamber. The primary antibody was then applied and incubated in the humid chamber for an hour. The slides were then washed three times in PBS for 5 minutes. The secondary antibody was then applied and incubated in a dark, humid chamber for one hour. The slides were again washed three times with PBS for 5 minutes. Afterwards, one drop of ProLong® Gold Antifade reagent with DAPI was applied, the coverslip was mounted and sealed with

transparent nailpolish. The slides were stored at 4 °C in the dark until usage and finally imaged with the Olympus FluoView FV1000 confocal microscope.

2.3.2 Extended protocol of IFA with NP40-extraction

NP40-extracted cells were prepared according to [100] by resuspending in 50 µL of NP40-buffer (10 mM Tris-HCl pH 6.8, 1 mM $MgCl_2$, 0.25% Tergitol) after initial washing steps. Cells were then spread on Superfrost Plus® slides (Thermo Scientific) and incubated for 3 to 5 minutes. Afterwards, the NP40-buffer was removed and 500 µL of 4% paraformaldehyde in PBS were added directly on to the slide. The cells were then fixed on the slide for about 10 minutes and the fixative was removed. Further steps of the protocol were as in point 2.3.1, starting with the washing-steps with 0.1M glycine in PBS.

2.3.3 Extended protocol of IFA with Microtubule-sieving treated trypanosomes

Instead of taking whole cells, the fraction P2 of the microtubule-sieving-procedure was taken (see section 2.4.3). **M**icro**T**ubule **S**ieving (MTS)-treated cells were then mixed with 4% paraformaldehyde to a 2:3 ratio, resulting in a 2.4% final concentration of formaldehyde. After fixing the resulting microtubule corset for about 30 minutes, the formaldehyde was removed. All further steps of the protocol were according to section 2.3.1, starting with the washing-steps in 0.1M glycine in PBS.

2.4 Subcellular Fractionations

2.4.1 Selective Permeabilization with Digitonin

In order to determine whether TbPH1 localizes to membrane-bound organelles, a selective permeabilization with digitonin was performed. [101] The technique results in multiple fractions with an increasing amount of digitonin in which more subcellular compartments are permeabilized with increasing detergent concentration, thus releasing their contents as a result. A western blot of the fractions are then probed with different organellar markers to determine the

possible organellar localizationtion of the studied protein. For one experiment with 10 fractions, 2 x 10^9 cells were grown and an additional 2 x 10^8 cells were used for a whole cell fraction. The cells were collected by spinning for 10 minutes at 1000 x *g*. and washed once in PBS. For the whole cell fraction, 1/11 of the cell cultures were transferred to a new Eppendorf tube and set aside. The rest of the cells were centrifuged (10 minutes, 1000 x *g*) and the pellet was resuspended in 1500 µL STE-NaCl buffer (25 mM Tris, pH 7.4, 150 mM NaCl, 250 mM sucrose, 1 mM EDTA). The cell suspension was divided into 10 aliquots, with 150 µL each. Each fraction was then brought to a final volume of 300 µL with STE-NaCl and an increasing amount of digitonin (see table 3).

Table 7: Cell lines of TbPH1 and corresponding selective drugs.

Sample-number	1	2	3	4	5	6	7	8	9	10
Digitonin [mM]	0	0.05	0.1	0.2	0.3	0.4	0.6	0.8	1.0	1.5

The samples were incubated at room temperature for 4 minutes, centrifuged at 14000 x *g* for 2 minutes and immediately put on ice. Samples were mixed with 5x SDS-PAGE sample buffer, boiled for 5 minutes and stored at -20 °C until their resolution on an SDS-PAGE gel and subsequent western blotting.

2.4.2 NP40-Fractionation

For isolation of the cytoskeleton, cells were extracted with IGEPAL (also known as Nonidet P-40). For each experiment, 10 mL of 1-2 x 10^7 cells were taken, collected by spinning down at 1100 x *g* for 10 minutes, transferred to a 1.5 mL Eppendorf tube and washed once in PBS. After another centrifugation (1100 x *g*, 10 min.), the cells were resuspended in 1 mL PEME+Complete protease inhibitor cocktail (100 mM PIPES-NaOH, 2mM EGTA, 0.1 mM EDTA, 1 mM $MgSO_4$, pH 6.9; buffer supplemented with 1x EDTA-free protease inhibitor cocktail [Roche]). A sample was taken for western blot analysis (Input). The cells were again centrifuged (1100 x *g* for 10 min.), the supernatant was aspired and the pellet was resuspended in 200 µL of PEME extraction buffer (PEME+Complete

supplemented with 0.5% IGEPAL). The mixture was incubated for 15 minutes at room temperature with gentle mixing. The lysate was then centrifuged at 3400 x *g* for 2 minutes at 4 °C. The supernatant (SN) was transferred to a fresh Eppendorf tube. The pellet (P), containing the IGEPAL-insoluble cytoskeleton, was spun again and the residual supernatant was discarded. Protocol adapted and modified from [100].

2.4.3 Microtubule-sieving (MTS)

This protocol was adapted from [102].

2.4.3.1 *MTS – the method*

Microtubule-sieving is a technique that uses the cage-like microtubule-corset of the parasite as a molecular sieve.

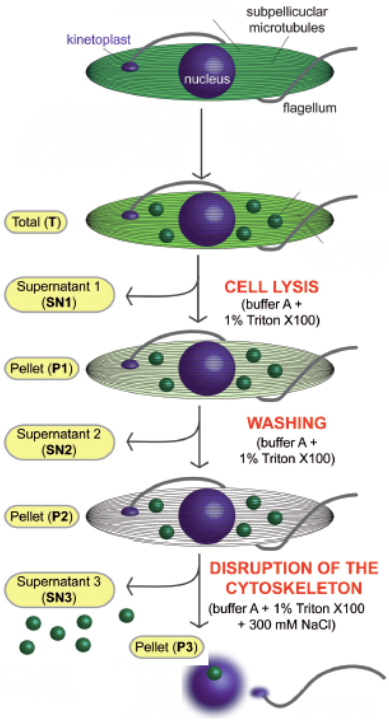

Figure 5: Process of Microtubule-Sieving, picture adapted and modified from [102]

Firstly, the plasma membrane is dissolved by TritonX-100 in a low-salt buffer, which leads cytoplasmic proteins to diffuse from the microtubule cage but trapping others that are in granules or other enclosed compartments. After several washing steps, the microtubules are then disintegrated by addition of a high concentration of NaCl, which releases the trapped contents of the cell.

2.4.3.2 *MTS – Cell Lysis and Washing Steps*

For small-scale experiments, 1-2 x 10^8 cells were taken. For larger-scale experiments, 5-10 x 10^8 cells were used. The cells were harvested by centrifuging them for 10 minutes at 1500 x *g*, the supernatant was aspired and cells were resuspended in 1 mL of PBS. The cells were then transferred to an Eppendorf tube, washed once with PBS and pelleted by centrifuging them for 30 seconds at 10000 x *g*.

All further steps were carried out on ice and centrifuges cooled to 4 °C. The cells were resuspended in 450 µL of Buffer A (20 mM Tris-HCl, pH 7.6, 2 mM $MgCl_2$, 10% glycerol, 250 mM sucrose, 1 mM DTT, MiliQ-water), lysed by adding 50 µL of 10% TritonX-100 and incubated for 10 minutes. A sample was taken for western blot analysis (Whole-cell lysate, WCL). The lysate was centrifuged 20 minutes at 20000 x *g* and the supernatant (SN1) was transferred to a new Eppendorf tube. For washing away the cytoplasmic proteins from the sample, the pellet was resuspended in 450 µL Buffer A and 50 µL of 10% TritonX-100 by passing through a 26G syringe and vortexing. A sample was taken for western blot analysis (P1) and the mixture was centrifuged for 20 minutes at 20000 x *g*. The supernatant was transferred to a new Eppendorf (SN2). The pellet was then resuspended in 450 µL of BufferA and 50 µL of 10% TritonX-100 by passing through a 26G syringe and vortexing. A sample was taken for western blot analysis (P2). This fraction (P2) was also the one taken for immunofluorescence assays of MTS-treated cells (see section 2.3.3).

2.4.3.3 *MTS – Disruption of microtubules*

To disrupt the microtubules, either 15 µL or 30 µL of a 5M NaCl-solution were added to get to an approximate final concentration of 150 or 300 mM NaCl, respectively. The higher salt concentration was used for preliminary experiments, the lower concentration was taken for most co-immunoprecipitation experiments. The mixture was incubated on ice for 30 minutes, with 26G-syringe passings and vortexing every 5 minutes. Afterwards, it was centrifuged for 20 minutes at 20000 x *g* and the supernatant was transferred to a new Eppendorf tube (SN3). This SN3-fraction was used further for immunoprecipitation-experiments. The pellet was resuspended in 450 µL BufferA and 50 µL of TritonX-100 for western blot analysis (P3).

2.5 Cell Cycle Investigation

2.5.1 DAPI (4',6-DiAmidino-2-PhenylIndole) Staining

Both procyclic and bloodstream form TbPH1-RNAi cells were taken and incubated with and without 1 µg/mL of tetracycline for 6 and 12 hours. About 10^7 of procyclic cells or 10^6 of bloodstream form cells were taken per slide, washed once in PBS and fixed for about 30 minutes in 4% paraformaldehyde in PBS. The cells were then washed again one time in PBS, resuspended in about 100 µL of PBS and were applied onto Superfrost Plus® slides. They were then incubated in a humid chamber for about 30 minutes. Excess fluid was poured off. In order to stain nucleus and kinetoplast of the cell, a drop of ProLong Antifade reagent with DAPI - (Life Technologies) was applied. The coverslip was mounted and sealed with transparent nail polish.

The stained cells were then observed with the Zeiss Axioplan 2 fluorescent microscope. The number of nuclei and kinetoplasts in each trypanosome was counted for at least 200 cells.

2.5.2 Propidium Iodide Staining and Flow Cytometry

Bloodstream form TbPH1-RNAi cells were taken and incubated for 6, 12, 24 hours and 3 days with and without 1 µg/mL tetracycline. About 10^6 of cells were taken and fixed overnight or longer in 70% methanol (v/v) in PBS. On the day of measurement, cells were washed twice in PBS, and then resuspended in PBS containing 5 µg/µL propidium iodide and 10 µg/mL RNAse A. After incubating the cells at 37 °C for 30 minutes in the dark, they were put to 4 °C until the time of measurement. FACS was performed with a Becton Dickinson FACSCantoTM II. Data was analyzed with the FACSDiVa software.

2.6 Immunoprecipitation of TbPH1

2.6.1 Crosslinking of V5-Antibody to Dynabeads

For crosslinking Protein G coated Dynabeads® (Thermo Scientific) to α-V5 Epitope Tag antibody (ThermoFisher scientific, 2F11F7), 1.5 mg of beads were washed two times with 200 µL of PBS-T20 (0.02% Tween20 in PBS). The beads

were then incubated with 5 µg of the V5 antibody and incubated overnight at 4 °C in constant rotation. Afterward, the beads were washed two times with 200 µL of PBS-TEA (0.1M TEA in PBS) and then incubated two times for 30 minutes with 200 µL of PBS-TEA-DMP (6 mg/mL DMP in PBS-TEA) at room temperature, rotating. The beads were washed two times for 5 minutes with PBS-TAE and 200 µL of quenching buffer (25 mM ethanolamine in PBS) were added, rotated for 5 minutes at room temperature and then washed once with PBS. Afterward, 200 µL of 1M glycine, pH 3 was added and incubated for 10 minutes rotating at room temperature. This step was repeated once more. The beads were then washed three times with the buffer used for immunoprecipitation (see 2.6.2) and stored at 4 °C until usage. In case of storage longer than a few days, 0.09% azide was added to the immunoprecipitation-buffer, in which the beads were stored.

2.6.2 Protocol of Immunoprecipitation

For small-scale experiments, approximately 1-2 x 10^8 of procyclic V5-tagged cells and 75 µg anti-V5 antibody-conjugated Dynabeads® were taken. For larger-scale experiments, about 1 x 10^9 cells and 375 µg Dynabeads® were used. In all cases, cells of the parental cell line SmOxP9 were taken as a negative control.

In order to reduce background of unspecifically binding proteins to Protein G Dynabeads®, cells were pre-fractionated by MTS-treatment of the cells and taking the SN3-fraction of the protocol (see section 2.4.3) in either high-salt (300 mM NaCl) or low-salt (~150 mM NaCl) conditions. The beads were washed three times in 1 mL of TX-IP-buffer (20 mM Tris-HCl, pH 7.7, 100 mM KCl, 3 mM $MgCl_2$, 0.5% TritonX-100 and cOmplete™, EDTA free protease inhibitor), before the lysate (SN3) was incubated with the washed, crosslinked anti-V5 antibody-Dynabeads (see section 2.6.1) for 24 hours at 4 °C, rotating. The next day, the supernatant was aspirated and kept for western blot analysis (Flow-through-fraction, FT). The beads were then washed three times with TX-IP buffer (double volume of original SN3-volume), and supernatants were also kept for western blot analysis (washings 1-3, W1-3). For elution, half of the original SN3-volume of elution buffer (50 mM glycine, pH 2.8) was added to the beads, incubated under constant agitation at 70 °C for 10 minutes and then neutralized with 10%

of the elution volume of neutralization buffer (1M Tris, pH 8.0). The elution-step was repeated one to two times.

2.7 Electrophoresis and Western Blotting

2.7.1 SDS-PAGE gel

For checking the expression of tagged proteins (C-terminal V5 and N-terminal HA-tag), SDS-PAGE was done according to the Laemmli protocol [103]. For the separation gel, either 10 or 12% acrylamide gels were used, further components were 375 mM Tris-HCl, pH 8.8, and 0.1% (w/v) SDS. For the stacking gel, a 5% acrylamide gel was used, containing 125 mM Tris-HCl, pH 6.8 and 0.1% (w/v) SDS. Gels were polymerized by adding 0.001% (v/v) TEMED and 0.1% (w/v) ammonium persulfate. SDS-PAGE buffer for electrophoresis was made of 25 mM Tris, 192 mM glycine and 0.1% (w/v) SDS. The gel was run at 60 V until the sample entered into the separation gel and then, voltage was increased to 120 V until the SDS-PAGE loading dye front of the gel reached the bottom. The Precisions Plus Protein™ Dual Color Standards (Bio-Rad) was used as a protein ladder.

For preparing *T. brucei* whole cell samples for electrophoresis, cells were counted, spun down (10 minutes, 1100 x *g*, room temperature), washed once and then resuspended in PBS to reach a concentration of 1 x 10^6 cells/µL. The appropriate amount of 5x SDS-PAGE sample buffer (10% (w/v) SDS, 100 mM Tris, pH 6.8, 30% (v/v) glycerol, 5% β-mercaptoethanol, 0.25% bromophenol blue) was then added to the cell suspension. The sample was then boiled for 10 minutes at 97 °C.

For western blot analysis, a volume corresponding to 1 x 10^7 cells was loaded. For gels intended for SYPRO® Ruby staining, an equivalent of 5 x 10^5 cells were loaded for controls and 2 x 10^7 cells for IP-elution samples.

For the final gel of the immunoprecipitation samples destined for SYPRO® Ruby-staining and subsequent excision of bands for Mass Spectrometry, a 12 well BOLT™ 4-12% Bis-Tris Plus gel (ThermoFisher scientific) was used. The Running Buffer used was the NuPAGE® MES SDS Running buffer (ThermoFisher

scientific). The gel was run at 200 V until the bromophenol blue dye front reached the bottom.

2.7.2. SYPRO® Ruby staining

After electrophoresis, the gel was placed in a clean container. About 100 mL of Fixing Solution (7% glacial acetic acid, 50% MeOH, MiliQ water) was added and incubated for 30 minutes at room temperature on an orbital shaker. This step was repeated once more with 100 mL of fresh Fixing Solution. Then, the gel was incubated with about 50 mL of SYPRO® Ruby solution and agitated on an orbital shaker overnight. The next day, the gel was placed in a new container and washed with 100 mL of Washing Solution (7% glacial acetic acid, 10% MeOH, MiliQ water) for 30 minutes on an orbital shaker. The gel was then rinsed three times for 5 minutes with MiliQ water before visualizing it with a ChemicDoc Imager.

2.7.3. Coomassie staining

After electrophoresis, the SDS-PAGE gel was placed in a container with about 100 mL of Coomassie staining solution (0.2% coomassie, 45% MeOH, 10% glacial acetic acid, MiliQ water) and microwaved for about one minute until the coomassie-solution boiled slightly. It was then incubated on an orbital shaker at room temperature for about 10 minutes. The coomassie stain was poured off and the gel was rinsed two times with distilled water. It was then put into Destain Solution (5% MeOH, 7% glacial acetic acid, MiliQ water), microwaved for 1 minute and incubated together with tissue paper on an orbital shaker until the background staining was sufficiently low. A picture was then taken with a ChemiDoc Imager.

2.7.4. Western blot analysis

After electrophoresis, the SDS-PAGE gel was placed in a Mini Trans-Blot Cell (Bio Rad) western transfer chamber for transfer onto a methanol-activated PVDF-membrane. The chamber was filled with transfer buffer (25 mM Tris, 192 mM

glycine, 0.1% (w/v) SDS, 20% (v/v) methanol) and transfer was done at 250 mA for 2 hours. The membrane was then blocked in 5% non-fat milk in PBS-T (0.05% (v/v) Tween20 in PBS) for either 1 hour at room temperature or overnight at 4 °C. The membrane was subsequently incubated for one hour in the primary antibody and washed three times for 5 minutes with PBS-T. Next, the membrane was incubated for one hour with the appropriate secondary antibody, washed again three times with PBS-T and then developed with the Clarity™ Western ECL Substrate kit. The membrane was then visualized with a ChemiDoc MP (Bio-Rad) using the accompanying Image Lab™ software.

3. Results and Discussion

The following experimental data is a result of an ongoing project. Many experiments will still need further investigation by different approaches as well as replication and verification of some parts. These cases will be indicated in the respective subchapters.

3.1 *In silico* studies of TbPH1

3.1.1 Structural features of TbPH1

Four general motifs can be distinguished on TbPH1 based on *in silico* analyses (Figure 6) [104, 105]: an N-terminal kinesin domain from amino acid (AA) 49 to 343, a coiled-coil region (AA 356-703), a pleckstrin homology domain (AA 689-846) and a homeodomain-like sequence (AA 868-959). Post-translational modifications include a methylation at a conserved arginine-residue among trypanosomatids (R540) and a phosphorylated serine at the beginning of the Homeodomain-like Domain (S868) [106, 107]. The kinesin domain suggests a function of TbPH1 binding to microtubules and perhaps also to moving along them as a motor (further discussed in section 3.1.2). The coiled-coil region that follows after the kinesin domain may mediate homooligmerization of the protein to either itself or to a different protein [59, 60]. The methyl-arginine site at R540 is situated within the coiled-coil region and could potentially influence this binding. The pleckstrin homology domain may allow TbPH1 to be involved in signalling [38], cytoskeletal organization [39], membrane trafficking [40] or phospholipid processing. It is surprising to find the homeodomain-like motif in TbPH1, as it usually has a function in binding DNA [62, 63] and the protein does neither have a signalling sequence for a nuclear nor mitochondrial import. A possible role for this domain could be in RNA-binding [108]. In this scenario, the phosphorylation-site at the beginning of the domain could be an on/off switch for the function of the homeodomain-like motif.

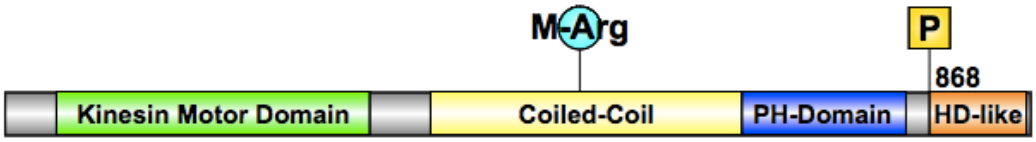

Figure 6: Structural features of TbPH1; R: Methyl-arginine; P: phosphorylation-site;

In addition, TbPH1 was found to be part of the palmitoyl-proteome of procyclic trypanosomes [109]. Palmitoylation is modification typically found in membrane proteins and can be reversible or permanent. This modification influences the interaction of the protein with lipids and proteins on a membrane [reviewed in 110]. The palmytoylation thus points at the possibility of an interaction of TbPH1 with lipids, possibly even at a function of anchoring membrane-bound organelles to microtubules.

3.1.2 Multiple alignment of TbPH1 WalkerA-domain with human KIF1

Figure 7: Multiple alignment of WalkerA-domain of TbPH1 with human KIF1 (red box).

The WalkerA-motif in the Kinesin Motor Domain generally consists of the following sequence: [AG]XXXXGK[ST]. This nomenclature means that at the first position, there is either an alanine or glycine, followed by any four amino acids, the fifth and sixth positions are glycine and lysine and the last amino acid is either serine or threonine. The multiple alignment of the WalkerA-domain of the human KIF1 with the kinesin domain of TbPH1 shows that there are mutations in the motif in the latter: the fifth position is mutated from a glycine to a proline and the last position is an arginine instead of serine or threonine (Figure 7, red box). This result means that most likely, the WalkerA-domain of TbPH1 is not functional and therefore, the catalytic activity of the Kinesin Motor Domain of TbPH1 is most likely abolished. However, as shown with the bacteriophage

terminases in the introduction (section 1.5), a deviation from the classical pattern of a Walker A motif can be still functional.

3.1.3 Multiple alignment of TbPH1 with other trypanosomatids

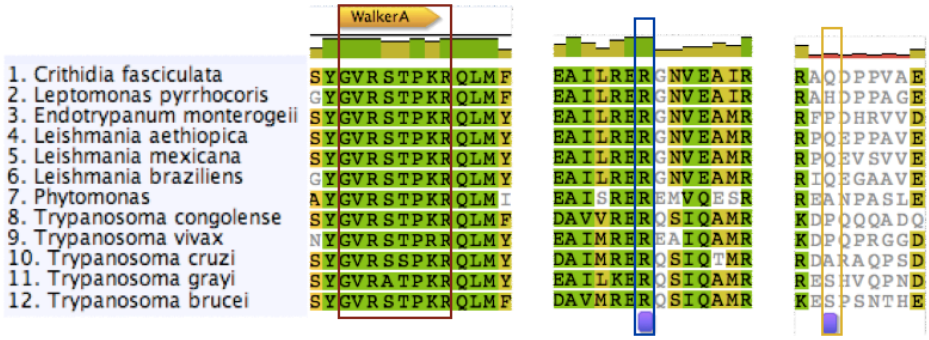

Figure 8: Multiple alignment of TbPH1 with other trypanosomatids

The multiple alignment of TbPH1 with homologs in other trypanosomatids reveals that these deleterious mutations in the WalkerA-domain are conserved (Figure 8, red box). This data could mean that even though WalkerA-domain is altered, this sequence is still essential for the function of the TbPH1. Furthermore, the position of the methyl-arginine (Figure 8, blue box) is conserved throughout trypanosomatids as well, suggesting that this post-translational modification may be fundamentally important to the protein's function. The phosphorylated serine (Figure 8, yellow box) is not conserved as the amino acids in its place in other trypanosomatid orthologs, except for *Trypanosoma grayi*, cannot be phosphorylated. Thus, the reported serine phosphorylation in the *T. brucei* otholog may be important only in this species or that this phosphorylation site is misannotated.

3.2 Cell line generation

3.2.1 Endogenous, C- and N-terminal tagging of TbPH1

After successful PCR-amplification of pPOT-V5-Hyg with primers for endogenous, C-terminal and N-terminal tagging of TbPH1, respectively, the former PCR-product was directly electroporated into the parental cell line SmOxP9. Positive clones were selected with hygromycin and expression of TbPH1-V5 was verified by western blot, with a monoclonal antibody against V5

(Figure 9, *left*). Afterwards, a pPOT –HA PCR-product was electroporated into the newly generated and verified TbPH1-V5 cell line for co-localization of the N-terminally HA tagged version of the protein. Positive clones were selected with blasticidin and expression of HA-TbPH1 was verified by western blot, with a monoclonal antibody against HA (Figure 9, *right*).

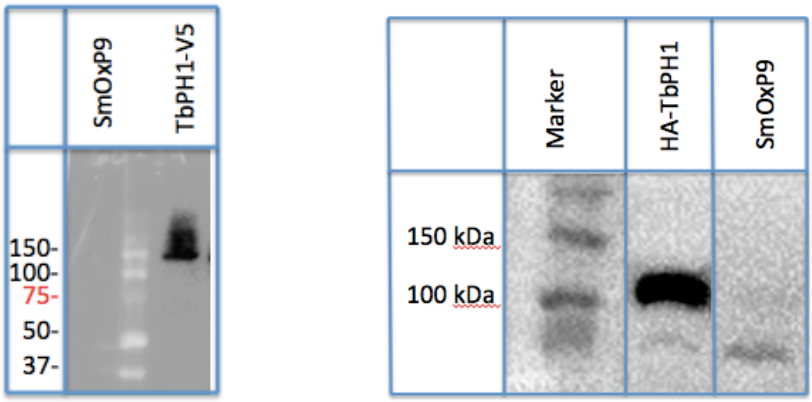

Figure 9: Western blot of verifying the expression tagged TbPH1; *Left:* C-terminally tagged TbPH1-V5 with SmOxP9 as negative control; *Right:* N-terminally HA-tagged TbPH1 with TbPH1-V5 as parental cell line and negative control.

3.3 Growth curves of PF and BS TbPH1-RNAi

For both procyclic and bloodstream form TbPH1-RNAi cell lines, the RNAi was induced via induction of tetracycline, thereby RNAi-silencing the expression of the protein TbPH1. In parallel, cells without the tetracycline-treatment were grown.

Each sample was done in three independent, biological replicates. Cell density was measured every day right before dilution. The knockdown of TbPH1 in procyclic *T. brucei* resulted in a slight growth-phenotype after the third day of induction (Figure 10). The depletion of the protein seems to be impairing in procyclic *T. brucei* fitness.

To confirm this finding, the growth curve in procyclics is going to be repeated for a longer duration to take samples for investigating knock-down efficiency by western blot analysis.

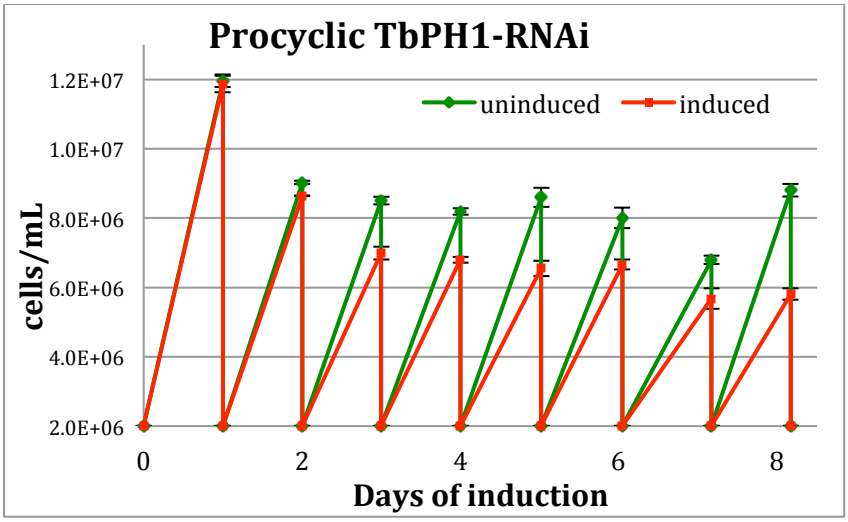

Figure 10: Growth-curve of procyclic TbPH1-RNAi. X-axis: Days of induction with tetracycline; Y-axis: Measured cell density in cells/mL.

Induction of TbPH1-RNAi by tetracycline in bloodstream form *T. brucei* resulted in a slight growth phenotype during the first 24 hours, turning into a severe growth-phenotype after the first day of the growth curve (Figure 11). Morphologically, a distinct "octopus"-phenotype was observed around day six of induction, which I interpret as the accumulation of multiflagellated cells (data not shown) This observation may indicate the involvement of TbPH1 in cell division as in its absence, cells seem to have difficulties to fully divide. On day eight of induction, the BSF trypanosomes seem to recover, most likely by acquired resistance to TbPH1 RNAi. However, this loss still needs confirmation by a repetition of the growth-curve and taking samples for checking protein-abundance by western blot. In general, the protein TbPH1 seems to be essential in the bloodstream stage. Interestingly, in a genome-wide RNAi-screen, TbPH1 is essential in procyclic but not in bloodstream form *T. brucei* [122], which does not agree with my findings.

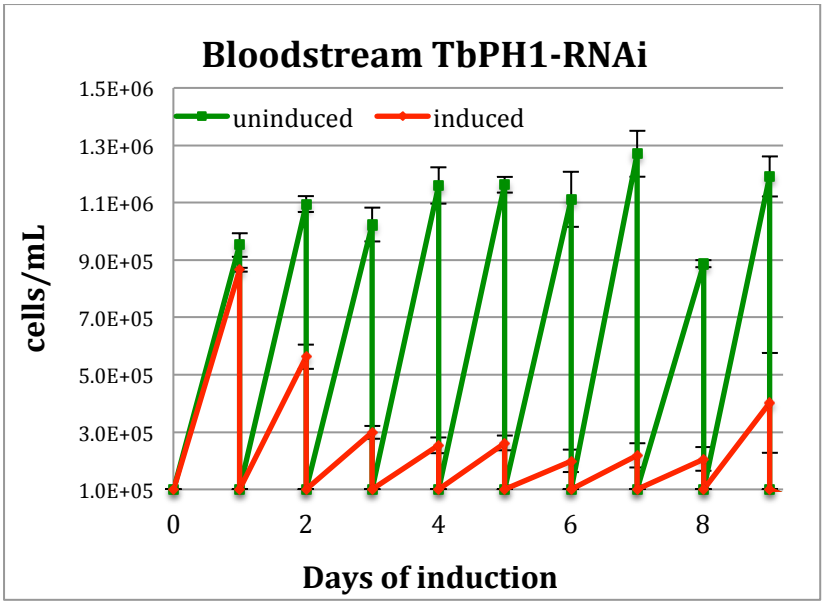

Figure 11: Growth-curve of bloodstream-form TbPH1-RNAi. X-axis: Days of induction with tetracycline; Y-axis: Measured cell density in cells/mL.

In order to see at which exact time point after RNAi-induction the bloodstream form start to exhibit differences in growth compared to non-induced cells, another short-term growth curve was conducted. For 24 hours, cell densities were measured every six hours (Figure 12).

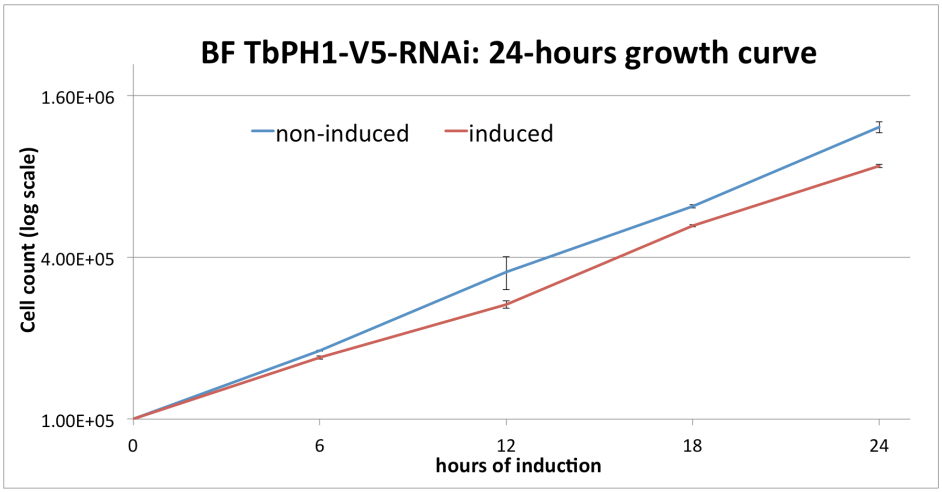

Figure 12: 24-hour growth curve of bloodstream-form TbPH1-RNAi. X-axis: Days of induction with tetracycline; Y-axis: Measured cell density in cells/mL.

After six hours of induction, the first differences in growth were already observed. As the trypanosomes were affected so early, it pointed to a possible contribution of TbPH1 to cell division. This finding was then further investigated

by examining potential alterations to the cell cycle upon depletion of TbPH1 (see next section).

3.4 Cell Cycle Investigation

3.4.1 DAPI-counts of RNAi-induced cells

For further clarifying the involvement of TbPH1 in the cell cycle of *T. brucei*, TbPH1-RNAi cells were induced and samples were taken at appropriate time points as revealed by the TbPH1-RNAi growth curves (See section 3.3). After DAPI-staining of methanol-fixed cells, cell cycle progression was analyzed by counting the amount of nuclei and kinetoplasts per cell. For bloodstream form *T. brucei*, a preliminary experiment of counting about 250 cells per time point at 6, 12, 24, and 48-hours induced and non-induced TbPH1-RNAi revealed an accumulation of 1N2K-cells and a simultaneous reduction of 1N1K-cells (Figure 13, *left*). In order to get statistical significance, the experiment was repeated with three biological replicates for selected time points. Again, an accumulation of 1N2K cells was observed with statistical significance (p-value less than 0.0001 in an unpaired t-test). This result indicates that indeed the depletion of TbPH1 affects cell cycle progression in bloodstream form *T. brucei* at an early point, which could mean that this is a direct and not a downstream effect.

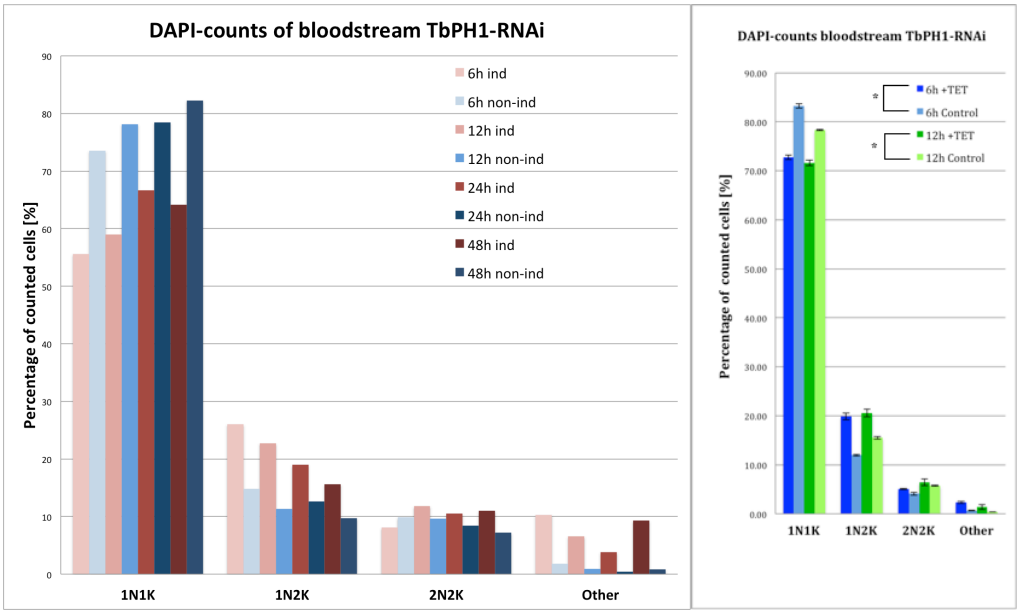

Figure 13: DAPI-counts of bloodstream form TbPH1-RNAi induced cells compared to non-induced cells after indicated induction-times. *Left:* preliminary DAPI-counts of one sample per time point. *Right:* DAPI-counts in triplicates for selected time points. * Unpaired t-test revealed a p-value of less than 0.0001 in between the induced and non-induced population.

DAPI-counts were then also performed on procyclic TbPH1-RNAi cells, which were induced for 4 days and compared to non-induced cells. (Figure 14).

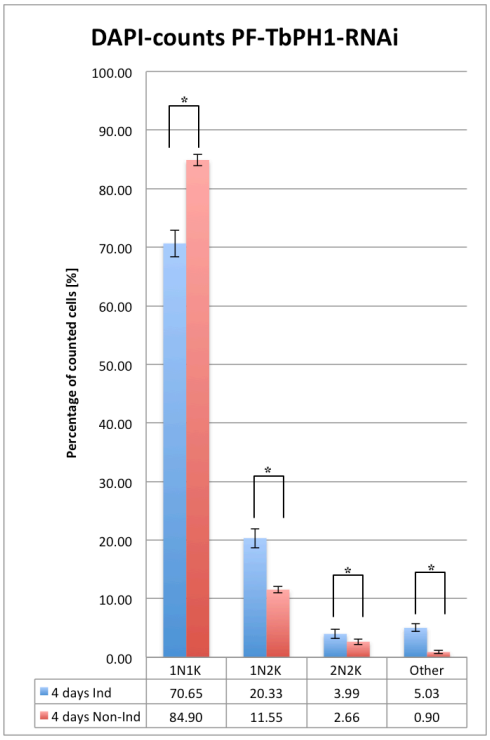

Figure 14: DAPI-counts of procyclic TbPH1-RNAi induced compared to non-induced cells after 4 days of induction. * Unpaired t-test revealed a p-value less than 0.0001 in between the induced and non-induced populations of 1N1K, 1N2K, 2N2K and other cells.

As seen in bloodstream form TbPH1-RNAi, more 1N2K and fewer 1N1K cells were observed in induced as compared to non-induced cells. This result could mean that the protein has a similar cell cycle progression role in both *T. brucei* life cycles stages.

The data suggests that cells get stuck at some point during nuclear S or G2-phase (using the terminlology introduced in section 1.3) by a potential delay in the progression of mitosis. It would make sense to argue that a process occurring around this point of time could be inhibited by silencing TbPH1. As described in the introduction, after the nuclear G2-phase occurs, the basal bodies begin to separate [117]. This process therefore could be possibly influenced by the silencing TbPH1. However, previous studies have shown that an inhibition of basal-body segregation rather leads to an accumulation of 2N1K and multinucleated cells than inhibiting the nuclear M-phase [111,112]. The exact reason for the accumulation of 1N2K cells still has to be further investigated.

3.4.1 FACS-measurement of bloodstream RNAi-induced cells

To confirm DAPI-stained cell counts, flow cytometry of propidium iodide stained cells was performed. Cells were taken in three biological replicates at the same time points used in the previous analyses. For the evaluation of the data, two gates were manually adjusted for each obtained sample, corresponding to cells in GO/G1 phase and G2 phase, respectively (Figure 15; see also Materials and Methods, section 2.5.2). The resulting tables show the calculated ratios of cells in G2 phase with duplicated nuclear DNA to cells in G0 and G1 phase.

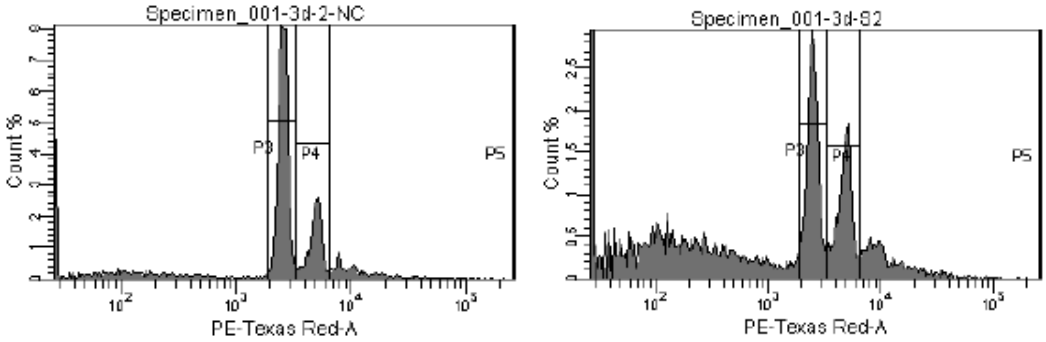

Figure 15: Sample of FACs analysis of propidium iodide staining of bloodform cells showing utilized gates and G2 accumulation.. P3: Gate for cells in G0 and G1 phase. P4: Gate for cells in G2 phase. *Left:* Uninduced control; *Right:* Tetracycline-induced sample.

By this flow cytometry assay one cannot easily distinguish between 1N1K and 1N2K cells due to the small size of the kinetoplast in comparison to the nucleus. The obtained data clearly shows a difference between induced and non-induced bloodform cells starting at the time point of 24 hours (Figure 16). When looking at the summary of the flow cytometry data, there is a trend to a higher DNA-content in induced samples at six and twelve hours observed. At 24 and 72 hours of induction, cells in G2 phase are generally higher in number in induced cells. These findings of the FACS-measurement confirm a role of TbPH1 in cell cycle progression of T. brucei. There seems to be an accumulation of G2 cells starting from 24 hours of induction. The data suggests that a silencing of TbPH1causes an error in the time frame after kDNA replication but before mitosis that leads to a delay of nuclear mitosis but does not inhibit it. (More about this topic will be discussed in chapter 5 – Outlook).

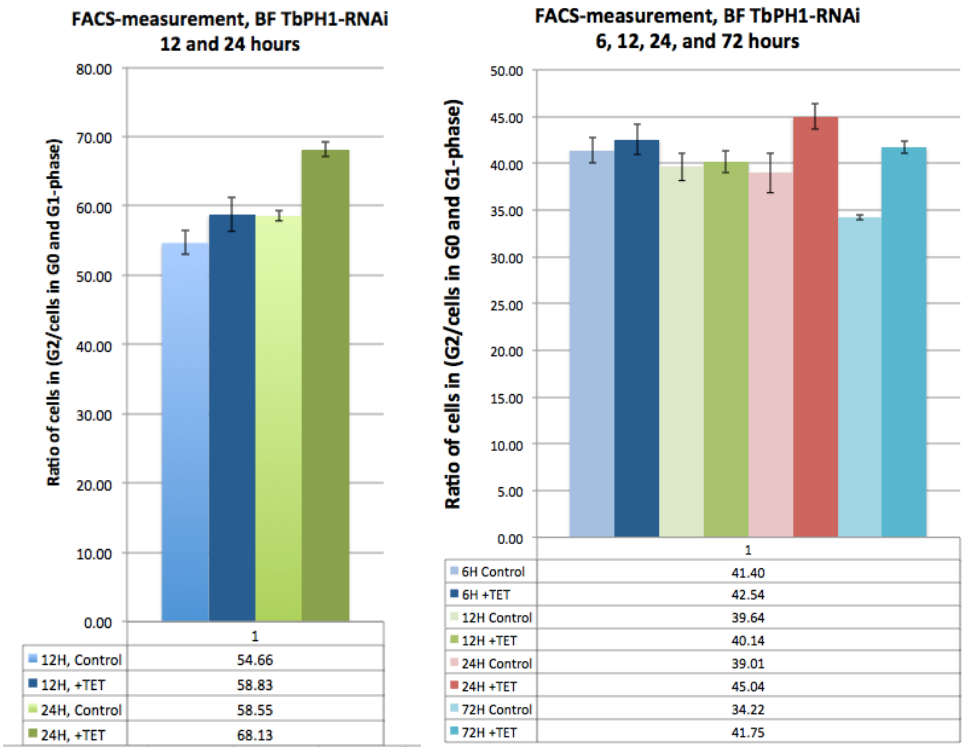

Figure 16: Summary of flow cytometry data of propidium iodide stained bloodform cells. Control: Negative control, uninduced cells. +TET: tetracycline-induced RNAi at indicated time. *Left*: preliminary, first FACS-measurement in triplicates. *Right*: FACS-measurement in triplicates of all obtained samples. Y-axis shows the ratio of cells in (G2 phase/cells in G0 and G1-phase).

3.5 Subcellular Localization of TbPH1

3.5.1 Localization of C- and N-terminally tagged TbPH1 in whole cells

In procyclic *T. brucei*, the localization of endogenous, C-terminally V5-tagged TbPH1 is concentrated in spots and throughout the cytosol (Figure 17).

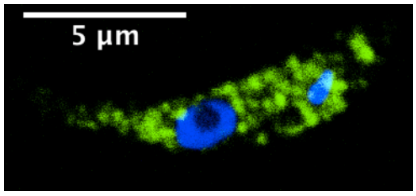

Figure 17: C-terminally tagged TbPH1 with V5 in procyclic *T. brucei.* Green signal: TbPH1-V5; Blue signal: DAPI-stain.

The N-terminal HA-tagged version seems to be more homogeneously spread throughout the cytosol, although there are spots, where the signal is more concentrated. (Figure 18, A). The more homogeneous spread of the signal could be due to some artefact of the primary antibody against HA, recognizing an additional epitope in procyclic *T. brucei*. This gets apparent when looking at the

verification of TbPH1-HA clones after electroporation, where an additional, faint band slightly below TbPH1-HA can be seen (Figure 9). When looking at the negative control of the IFA with the parental cell-line SmOxP9 (Figure 18, B), there is indeed some background seen that could account for the pattern. However, the N-terminal tagging has to be repeated with a different tag or anti-HA antibody to get a clearer picture without this background.

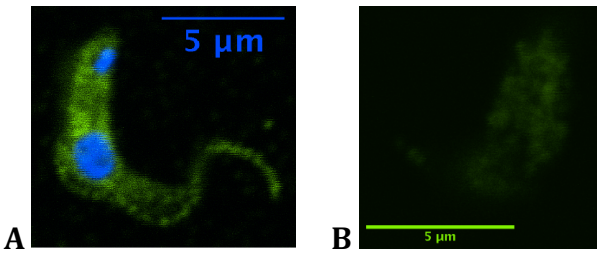

Figure 18: *A:* N-terminally tagged TbPH1 with HA in procyclic cells; *B:* Negative control of IFA with same treatment as in A with the parental SmOxP9 cell line.

The localization of MTS-treated cells reveals an accumulation of TbPH1 between the kinetoplast and the nucleus and a dot-like pattern along the flagellum (Figure 19). This could point to localization at the **F**lagellum **A**ttachment **Z**one (FAZ). To confirm this hypothesis, a co-localization with a marker for the FAZ is going to be done in a future experiment.

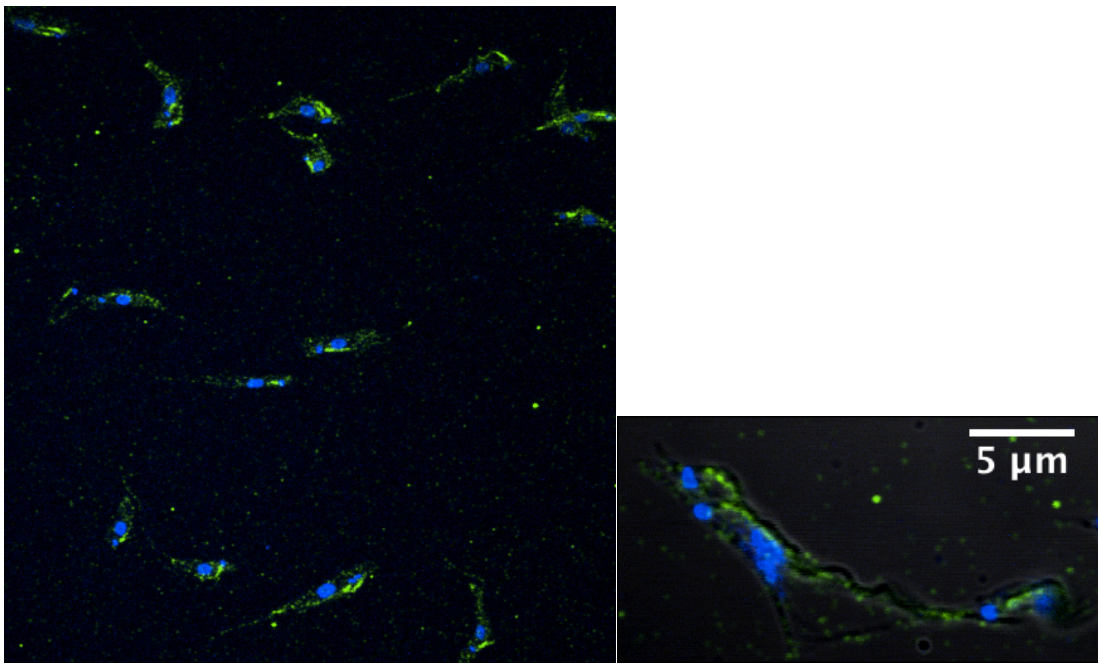

Figure 19: IFA of MTS-treated, procyclic *T. brucei*, C-terminal V5-tagged TbPH1;

In long slender bloodform *T.brucei*, the C-terminal, V5-tagged version also exhibits a spot-like pattern throughout the cytosol (Figure 20). Here, a 3D model constructed from the obtained confocal z-stack was performed using the Imaris software (Bitplane) in order to see the three-dimensional distribution of the protein (Figure 20, A).

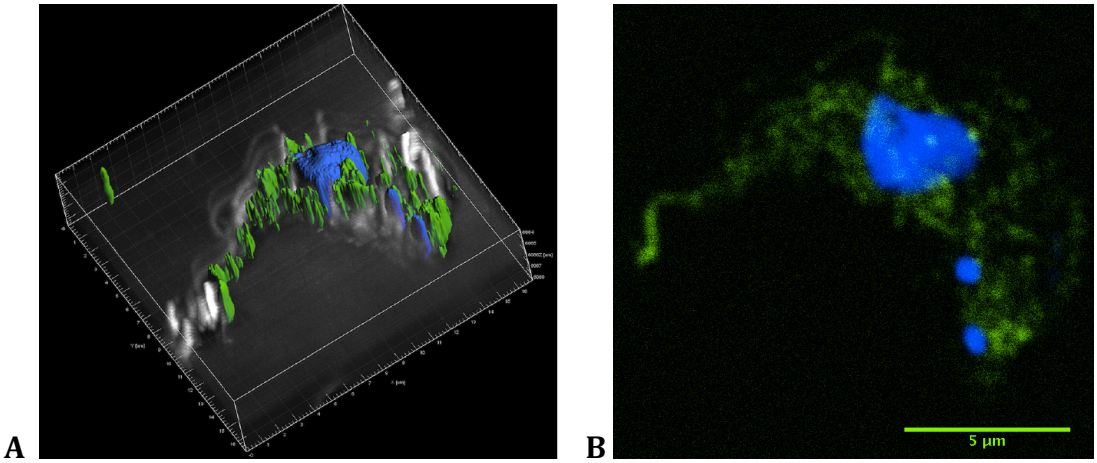

Figure 20: Localization of TbPH1-V5 in bloodstream form *T. brucei*; *Left*: 3D model of confocal z-stack; *Right*: A middle focal plane from the z-stack used for the 3D-model on the left.

The signal of the N-terminal HA-tag is somewhat similar to that in procyclics, also being more homogeneously spread throughout the cell as compared to the C-terminally, V5-tagged version (Figure 21). However, the pattern does still seem punctate. The DAPI signal is out of focus in this picture, which potentially can influence the observed pattern. As with the procyclics, the discrepancy between the N- and C-terminal tags should be addressed by using a different epitope for anti-HA antibody species.

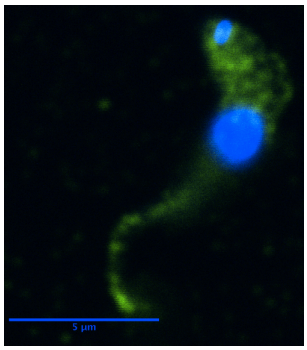

Figure 21: Localization of HA-TbPH1 in bloodstream form *T. brucei*.

3.5.2 Co-localization of TbPH1 with diverse markers in the whole cell

The punctate pattern of TbPH1-V5 may be due to its localization within an organelle or attachment to microtubules. To test this hypothesis, the protein was co-localized with various proteins or fluorescent dyes serving as organelle markers in procyclic cells. Tested were the mitochondrion (Mitotracker), endoplasmic reticulum (BiP), acidocalcisome (TbVP1), stress-granules (SCD6) and microtubules (α-tubulin; see Figure 22).

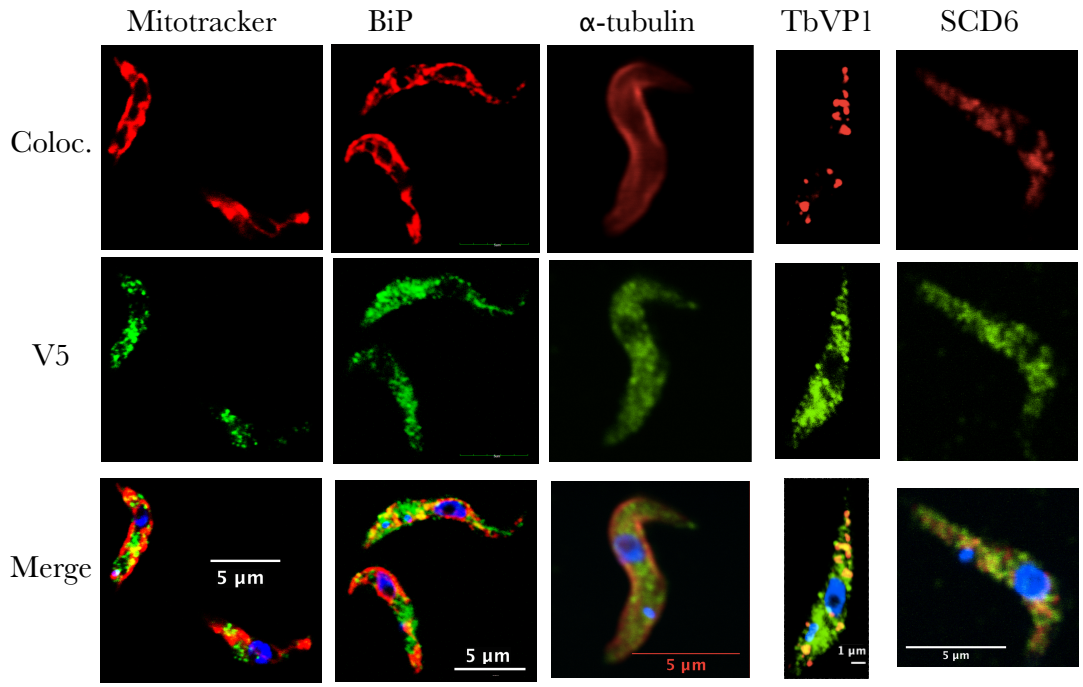

Figure 22: Co-localization of TbPH1-V5 in procyclic *T. brucei* (green) with various intracellular markers (red); Mitotracker: mitochondrion; BiP: endoplasmic reticulum; α-tubulin: cytoskeleton; TbVP1: acidocalcisome; SCD6: stress granules; Merged pictures also contain DAPI-stained nucleus and kinetoplast;

No complete co-localization with any of the tested compartments was observed. A partial co-localization was seen in case of the acidocalcisome, in traces also for the mitochondrion and the endoplasmic reticulum. When looking at the co-localization of TbPH1 with the mitochondrion and the endoplasmic reticulum, the protein seems to be enriched in the space that is not occupied by either of these organelles.

3.5.3 Co-localization of TbPH1 in microtubule-sieved cells

After an IFA of microtubule-sieved cells had revealed that TbPH1-V5 accumulates in between kinetoplast and nucleus (Figure 19) and possibly along

the FAZ, additional co-localizations were done on the P2-fraction (See section 2.4.3 for method) of MTS-treated, procyclic cells (Figure 23). Markers for stress-granules were used to confirm the functioning of the method. The co-localization of TbPH1 with microtubules (α-tubulin) revealed that the protein seems to be either overlapping or directly adjacent to microtubules. However, the signal for α-tubulin was relatively intense, which might conceal a subtle difference between the genuine co-localization and TbPH1 being directly adjacent to the microtubules. A co-localization with the paraflagellar rod showed no overlap. Unfortunately, an attempt to co-localize TbPH1 with FAZ did not work. However, this experiment is planned to be repeated in the future.

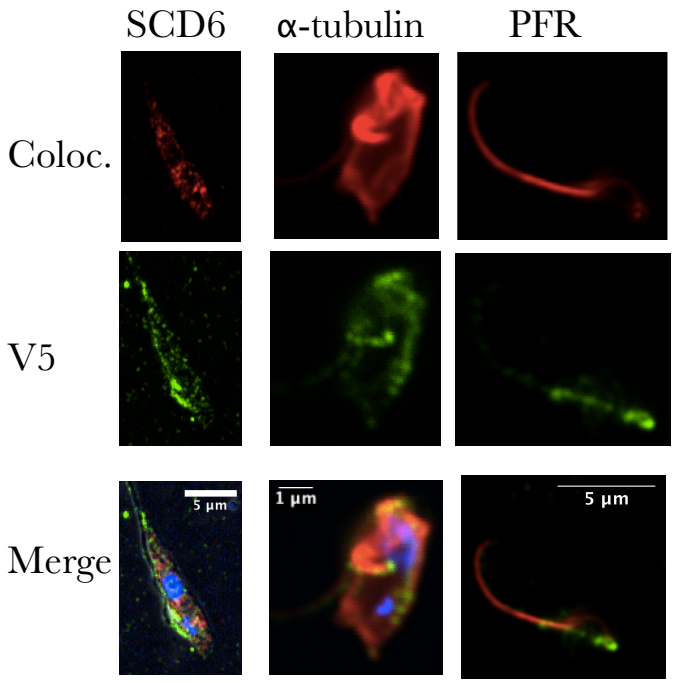

Figure 23: Co-localization of TbPH1-V5 (green) in procyclic *T. brucei* with various markers on P2-fraction of microtubule-sieving treated cells. SCD6: stress granules; α-tubulin: cytoskeleton; PFR: paraflagellar rod;

3.6 Biochemical Fractionations

In order to gain further insight into the localization of TbPH1, several biochemical subcellular fractionations were done with the procyclic, C-terminally V5-tagged TbPH1 cell line.

3.6.1 NP40-fractionation

A treatment of cells with the NP40 detergent extracts the cell membrane and thus, releases the cytosolic proteins from the cell. What is left in the pellet is the cytoskeletal fraction. Thus, with this technique, one can distinguish between cytosolic proteins in the supernatant (SN) and cytoskeletal proteins in the pellet. As can be seen in Figure 24, TbPH1-V5 is predominantly present in the supernatant, suggesting TbPH1 is a cytosolic protein. The faint band in the pellet can be explained by a small amount of residual supernatant in the pellet-fraction. The marker for the cytoskeleton, α-tubulin, is enriched in the pellet fraction, although there is a small amount in the supernatant, too. This result is maybe due to soluble α-tubulin-monomers that show up in the cytosolic fraction [113]. To test the previously observed partial co-localization of TbPH1 with acidocalcisomes in IFAs, the western membrane was then also probed with the α-TbVP1 antibody, a marker of the organelle. It was found that the marker for acidocalcisomes goes to the cytosolic fractions as well.

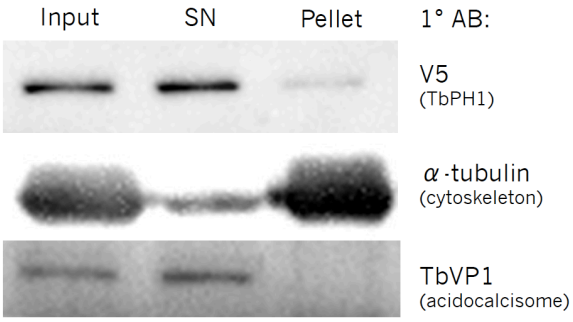

Figure 24: Western blot of NP40-fractionation with procyclic, C-terminally tagged TbPH1-V5.

Afterwards, cells were treated with NP40 and prepared for IFAs, with primary antibodies against V5 (green, TbPH1) and TbVP1 (red, acidocalcisome). The observed populations ranged from cells containing a bit of signal for TbPH1-V5 to being completely depleted of the signal (Figure 25). The differences could be due to completely and only partially NP40-extracted cells.

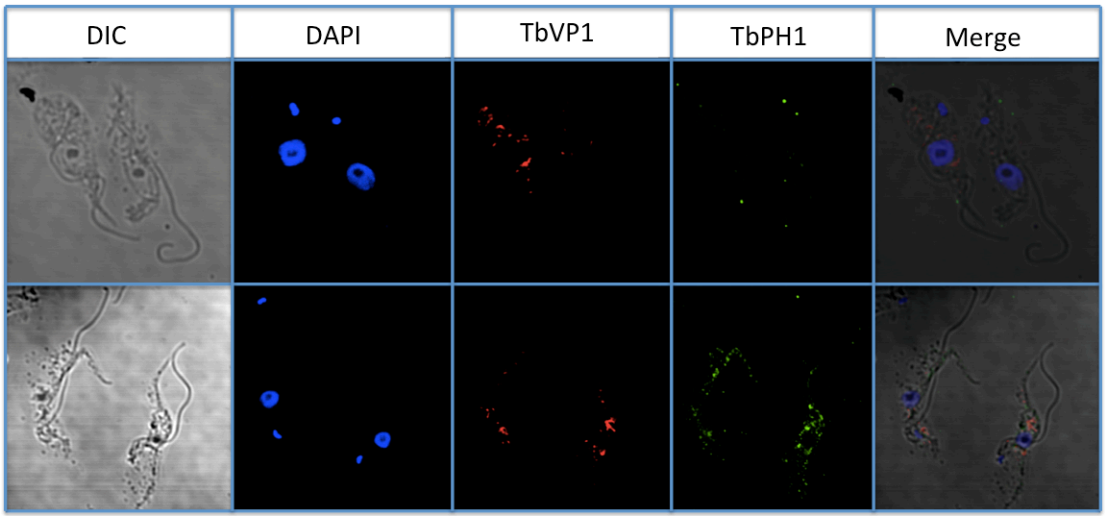

Figure 25: IFA of NP40-extracted procyclic *T. brucei*, with TbPH1-V5. TbVP1: marker for acidocalcisome (red) TbPH1-V5 (green).

3.6.2 Digitonin-fractionation

As being both in the supernatant-fraction of the NP40-fractionation does not clarify if TbPH1 is indeed co-localizing with acidocalcisomes, a selective permeabilization with digitonin was performed. Procyclic TbPH1-V5 cells were incubated with increasing concentrations of digitonin. These fractions were subsequently probed for the presence of enolase (as marker for the cytosol), mtHSP70 (mitochondrial matrix) and TbVP1 (acidocalcisomes) (Figure 26).

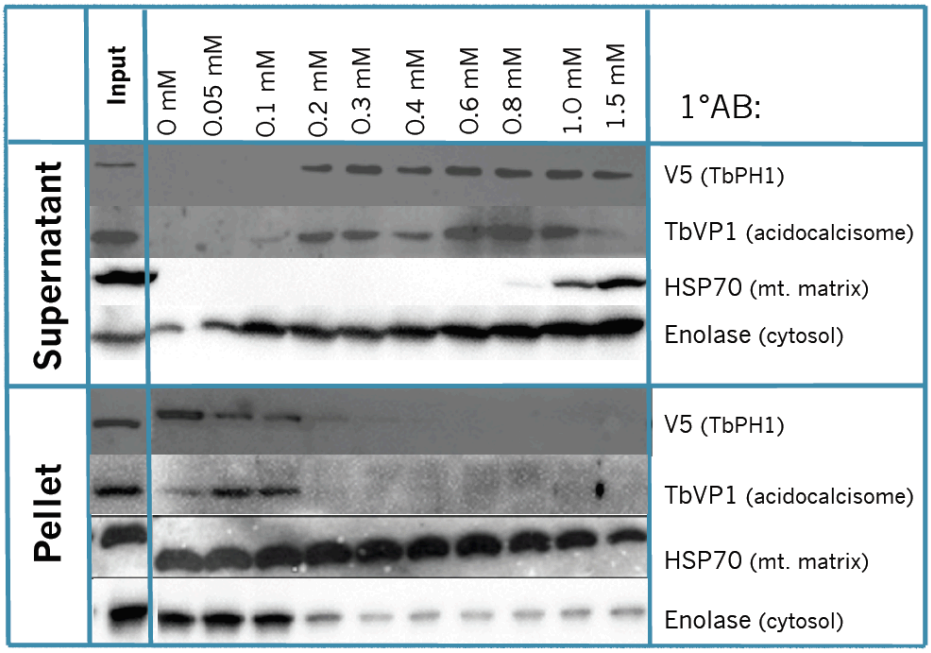

Figure 26: Western blot of Digitonin-fractionation. Procyclic TbPH1-V5. Used markers for co-localization indicated.

TbPH1 gets released from the cell at a concentration in between 0.1 and 0.2 mM digitonin. Enolase on the other hand, is in the supernatant from the very beginning, as expected for a cytosolic protein. This result means that TbPH1 is most likely not cytosolic and seems to be either in or perhaps even associated with some intracellular compartment. TbPH1 is definitely not in the mitochondrial matrix as proteins situated there are released by a higher concentration of digitonin. The acidocalcisome protein TbVP1 appears to have quite similar pattern to the TbPH1 at first. However, there are slight differences, such as the presence of a faint band in the 0.1 mM fraction in the case of TbVP1 that is not observed for TbPH1. That means that the protein TbPH1 is most likely not situated in acidocalcisomes either. With this experiment, some localizations of TbPH1 were excluded. However, the exact position of the protein could not be pinpointed.

3.6.3 Microtubule-sieving

The technique of microtubule-sieving was initially performed in order to further investigate the localization of TbPH1. This technique had been formerly used by the Susanne Kramer laboratory to purify stress granules [102]. These granules were retained inside the cage if the microtubule corset and released when microtubules were disintegrated at a high-salt concentration. Interestingly, TbPH1-V5 was among the proteins retained after MTS-treatment, albeit not enriched in stress granules [102]. MTS was performed using the TbPH1-V5 cell line to verify this result. The protein was retained inside the cell in case of an intact microtubule-corset (Figure 27, P1 and P2-fraction) and released when microtubules were depolymerized with a high-salt concentration (Figure 27, SN3-fraction). This result could either mean that TbPH1-V5 is either situated in some kind of granule or organelle, which is in agreement with the digitonin-fractionation results, or that it is very tightly associated with microtubules and only disassociates when the microtubule themselves are disassembled. The microtubule-sieving data is surprising when comparing it to the result of the NP40-fractionation as the latter lead to the conclusion that TbPH1 is not associated with microtubules.

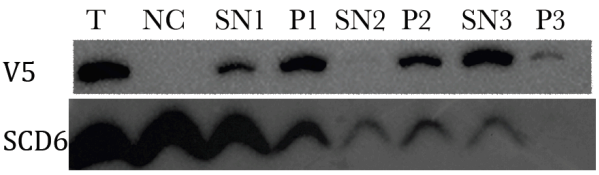

Figure 27: Western blot of preliminary MTS-fractionation. V5: TbPH1-V5; SCD6: Marker for stress granules.

For verifying that the method itself had worked, the western membrane was also probed with a marker for stress granules (α-SCD6). This experiment was performed on unstarved *T. brucei*, thus lacks SCD6-containing stress granules. However, the pattern localization pattern of SDCD6 in this experiment (Figure 27 lower panel) matched that of the unstarved samples done by Fritz *et al.* study [102; *c.f.* Figure 3, A].

As the MTS-method resulted in almost all TbPH1-V5 being retained SN3-fraction, which had been subjected to several washing steps, the purity of the MTS-fractions was tested to determine if this method would be suitable for co-immunoprecipitation experiments to identify protein binding partners. To this end, all fractions from the MTS-procedure were run on a 10% SDS-PAGE gel and subsequently stained with coomassie stain to be able to estimate the grade of purification achieved. As can be seen in Figure 28, a substantial amount of protein is washed away in the SN1 and SN2-fractions and the left-over pellet

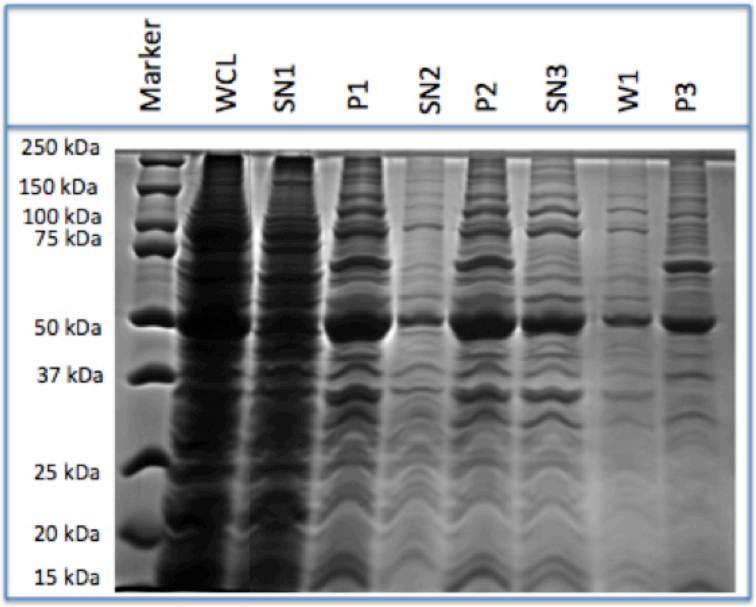

Figure 28: Coomassie-stained 10% SDS-PAGE of MTS-fractions. WCL: Whole cell Lysate; NC: Negative Control: parental cell Line SmoxP; SN: Supernatant, P: Pellet; W: Washing-step;

after disassembly of microtubules (fraction P3) contains a lot of protein, too. When comparing the amount of protein in the TbPH1-V5 containing, final fraction (SN3) with the whole cell lysate (WCL) it gets clear that indeed, this method is suitable to pre-purify TbPH1-V5 for subsequent immunoprecipitation.

3.7 Co-Immunoprecipitation of a kinesin with TbPH1

To identify interaction partners of TbPH1, it was immunoprecipitated via the V5-tag in the procyclic TbPH1-V5 cell line. A pre-purification was achieved by the MTS-method (see section 2.4.3).

The SN3-fraction of this procedure was then incubated with Dynabeads with conjugated antibody against V5.

3.7.1 Time-course for Optimization of Dynabead-incubation

In preliminary co-immunoprecipitations with 0.2 mM digitonin permeabilization, it was observed that short incubation-times of cell lysate with Dynabeads, most of TbPH1-V5 was found in the flow-through. However, too long incubation times may be a source of background due to unspecific binding of proteins to the Dynabeads. To keep the balance in between efficient protein pull-down and minimizing the background of unspecific binding, a time-course for Dynabead-incubation with cell lysate was performed (Figure 29).

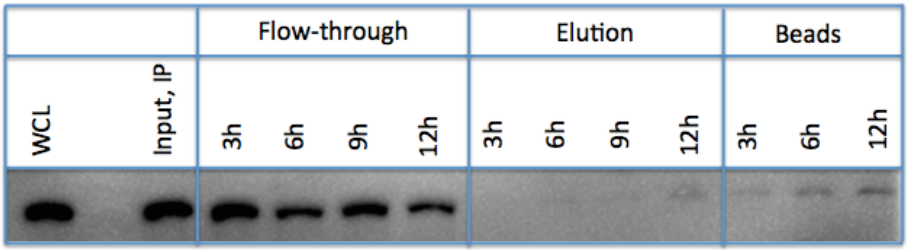

Figure 29: Immunoprecipitation time-course for optimization of duration of Dynabead-V5 antibody incubation with MTS SN3 fraction. Indicated times correspond to incubation times, used antibody for western was anti-V5.

The time course revealed that the amount of TbPH1-V5 being pulled-down was indeed dependent on the incubation time of cell lysate with V5 antibody conjugated Dynabeads. Furthermore, it was observed that it was necessary to incubate the cell lysate at least for 12 hours to pull-down a minimal amount of TbPH1-V5. The incubation time was then decided to be prolonged to 24 hours as this improved TbPH1-V5 pull-down efficiency, albeit still not binding all antigen (Data not shown but an example of this prolonged incubation time of 24 hours can be seen in Figure 30).

3.7.2 Pre-Purification and Co-IP to obtain MS-samples

After optimizing the pull-down conditions, the experiment was scaled-up and performed once more in order to get samples for mass spectrometry-analysis of interaction partners. The final pre-purification method was decided to be MTS-sieving and not a digitonin-fractionation, as MTS-sieving gave a purer fraction of TbPH1. In addition, the incubation-time of the SN3-fraction with V5-coated

dynabeads was chosen to be 24 hours like in the preliminary time-course experiment to maximise the amount of pulled-down protein. In figure 30, the western blot for checking the result of the pre-purification can be seen. The amount of TbPH1-V5 lost in purification steps (SN1, SN2, W1 and P3) was even less than in the preliminary experiments.

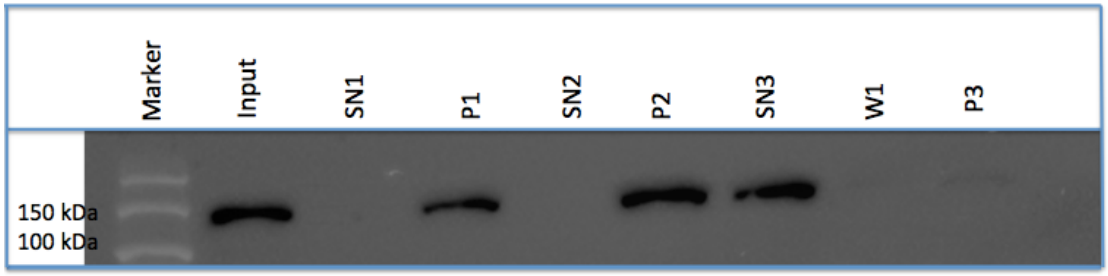

Figure 30: Western blot of pre-purification for immunoprecipitation. SN: Supernatant; P: Pellet; W: Washing-step;

The SN3-fraction of the MTS-treated cells were then incubated for 24 hours with V5 antibody conjugated Dynabeads. A western blot of the immunoprecipitation-samples was then performed in order to make sure that the right protein had been pulled-down (Figure 31). Out of curiosity, the western membrane was also probed with an antibody against α-tubulin to see if TbPH1 is associating with microtubules. Interestingly, not even a faint band of α-tubulin was observed in the eluate of the co-immunoprecipitation. However, this does not mean that TbPH1 is not associating with microtubules at all. There is still the possibility that it is binding to either β-tubulin or other isoforms of tubulin.

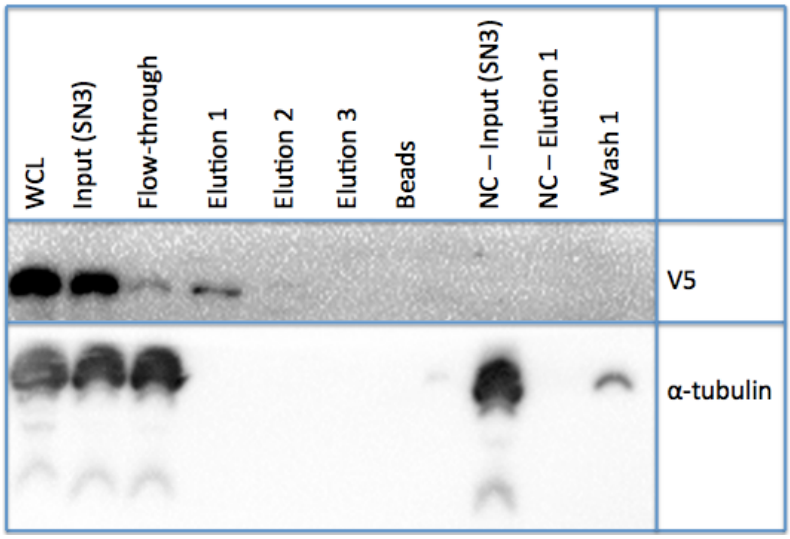

Figure 31: Western blot of TbPH1-V5 immunoprecipitation fractions. WCL: Whole cell lysis; Elution with 50 mM Glycine, pH 2,8; SN: Supernatant; NC: Negative Control (SmoxP parental cell line without V5-tagged TbPH1);x

3.7.3 SYPRO® -Ruby gel of Co-Immunoprecipitation

The eluates of the IP where run on a gel and SYPRO®-Ruby-stained. In high-salt conditions (300 mM NaCl), there were 2 major apparent bands observed that were not present in the negative control, which was the parental cell line SmoxP without V5-tagged TbPH1 (Figure 32). Surprisingly, the bands look bigger than the ones in the final co-immunoprecipitation, which could be due to a effect of the high salt-concentration (Figure 33). No band for endogenous TbPH1 was seen, which means that either the bands were not resolved in the gel or that TbPH1 is not interacting with itself. Both bands in the gel appear to be of equal intensity, which might point to a stoichiometric relationship between the two proteins.

To investigate whether more *bona fide* interaction partners are missed in high-salt conditions, a low-salt condition (150 mM NaCl) co-immunoprecipitation was performed and ultimately taken for the final co-immunoprecipitation destined for mass spectrometry.

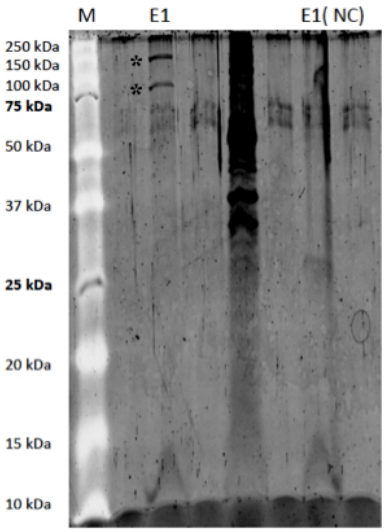

Figure 32: SYPRO®-Ruby stained 10% SDS-PAGE gels of co-immunoprecipitation eluate. Preliminary high-salt eluate experiment; additional bands as compared to negative control indicated with an asterisk (*) M: marker; E1: elution 1; NC: negative control; **Bold** written kDa-sizes correspond to dark bands in the marker.

Running the eluates of the final co-immunoprecipitation on a gel, SYPRO®-Ruby staining showed two bands that were not present in the negative control (Figure 33). The two bands in question – one above 100 kDa and one in between 98 and

62 kDa – were then excised from the gel and sent for mass spectrometry analysis. In order to confirm the outcome of the co-immunoprecipitation and clarify the possibility of more interaction-partners, another co-immunoprecipitation is planned to be done in the future.

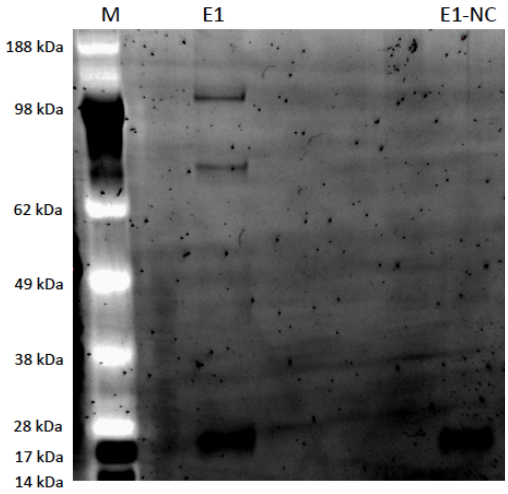

Figure 33: *Right*: Final low-salt eluate, run on precast-gradient gel and stained with SYPRO®-Ruby, used for excision of bands for sending for mass spectrometry. M: Marker; E1: elution 1; NC: Negative control (parental cell line SmoxP without V5-tagged TbPH1)

3.8 Mass Spectrometry Data

Mass spectrometry analysis revealed the identity of the two excised bands of the eluate from the co-immunoprecipitation. The upper 110 kDa band was the bait TbPH1, which was expected. The lower 75 kDa band was Tb927.9.15470, which is annotated as a putative kinesin 11 (KIF11) in the TriTrypDB online database of the *T. brucei* genome [104]. No other proteins were identified in this sample. The band from around 110 kDa contained mainly TbPH1 (37 peptides) and to a minor extent TbKIF11 (9 peptides, see Figure 34) and the excised band from the size around 75 kDa contained mainly KIF11 (41 peptides) and to a smaller extent TbPH1 (5 peptides)

To confirm this result, another Co-IP of TbPH1-V5 is planned as well as an IP of tagged TbKIF11.

Sequence of TbKIF11 with peptide sequences found via MS in 110 kDa band

MADMKKVTVAVRVRPILRDGISQAHVQEKFELEAIRRTGDTTLKVELERPGEPTRGSA
FTFDHIFDQESTQLDVYDEAVADLVDMSLTGANSTILAYGQTGSGKTFTVLGDVKPNP
LEDDLLTKDSGMFLRVLSDLMEYKRRQLARGFHVVVGLSCVEIYNENIRDLFGGTPNS
PPPSIKAVMIGEEVLLPSLIIKEMTSLQAVFSEIQLAISRRKSRSTEANAVSSRSHCLFLID
ILQQSTTAPAPSLTAILQTKKGTKDVEAKRISTLSGISNKNGAPIELKPGELPFDGMVYR
LQGQKEPIYGSKILLADLAGSEKISRSGVTGEGLAEATAINSSLTALGNVVHSLHEGGYV
SYRTSNLTRLLKPTFSHPNSRVLLLSQVSPTQMTFDETISTLHFANKVKAMKVTTSTG
MEADKIQFEYVEAGRTYDGLLADLRLFAVEQQTKVGVIRRRCRQNDGLFYAPLPSGRA
GTRERRQAFIESIGANKAATEEREAGKVARAREREAAAAWEEELRRKRKDGAESAAATHA
QLLREAKEGLAAEEKAVKHQAMQEVQHAQAAGAAKLQAEEEASRALLLGRFAQVMS
DFCRARLQEAARVEEEISRELNSTRMASSSGGNGSGAASEVPVEDLEYAVSCWGHSIA
KKFYTNCAELRELQLQMCMIGRSCLTMERWKAEHVGTA

Figure 34: Peptides found in the ~110 kDa-band of Co-IP TbPH1-sample of MS-data highlighted in yellow.

3.9 TbKIF11

3.9.1 Localization of TbKIF11

In 2016, Dean *et al.* started a project to localise every trypanosome protein in the genome [118]. The approach works by tagging the proteins C- and N-terminally with the fluorescent tag mNeonGreen and a subsequent visualization by microscopy. The pictures and determined localizations are then uploaded to the online-database www.tryptag.org, where the obtained pictures can be downloaded [118].

Localization of N-terminal mNeonGreen-tagged TbKIF11 (Tb927.9.15470) on tryptag.org [118], the protein seems to be spread unevenly throughout the cytosol (Figure 35, *left*). When comparing the localization of TbPH1 and TbKIF11, the patterns of the two proteins does not appear to be the same at first (Figure 35, *c.f. left* and *right*). To investigate this further, tagging of TbKIF11 is planned in order to do co-localization studies with TbPH1.

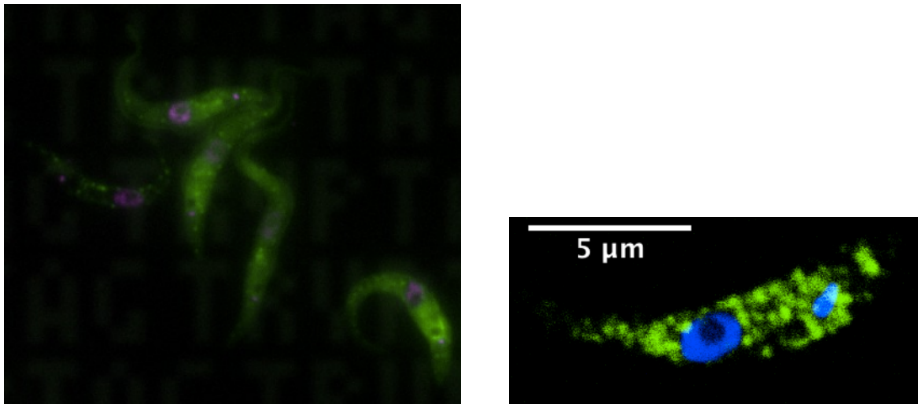

Figure 35: *Left:* Localization of N-terminally mNeonGreen-tagged TbKIF11, adapted from tryptag.org [118]; *Right:* Localization of TbPH1;

3.9.2 Motifs contained in putative TbKIF11

In order to find out about contained motifs in the putative TbKIF11, the sequence of putative TbKIF11 was submitted to the SMART (Simple Modular Architecture Research Tool) database [120, 121]. The database found one domain, called KISc (AA 4 - AA 415), which is a kinesin motor, catalytic domain and ATPase. It is predicted with high confidence to be a microtubule-dependent molecular motor, perhaps playing a role in intracellular transport of organelles and in cell division. A potential role of TbPH1 in regulating the function of TbKIF11 could imply a role in mitosis and explain the impact of TbPH1-silencing on the cell cycle.

4. CONCLUSIONS

The structural features of TbPH1 suggest that the protein can bind to microtubules. The coiled-coil region points at an interaction with itself or a different protein [59, 60]. The pleckstrin homology domain may allow TbPH1 to be involved in signalling [38], cytoskeletal organization [39], membrane trafficking [40] or phospholipid processing. The palmitylation hints at an interaction of the protein with lipids, possibly even at anchoring membrane-bound organelles to microtubules. The multiple alignment of the Walker A-domain then revealed that the kinesin domain is most likely not working as a motor, although this finding still has to be tested *in vivo* as even deviant Walker A-domains can potentially fulfill catalytical function [117]. As revealed by the growth curves of the knock-down of TbPH1, the protein is essential in long slender bloodstream form and procyclic *T. brucei*, albeit to a lesser degree, which might be due to a difference in RNAi efficiency. In both, bloodstream and procyclic stage, there appears to be an involvement of TbPH1 in the cell cycle, leading to an accumulation of 1N2K cells in the first twelve hours of RNAi-induction in the case of bloodstream form *T. brucei*. FACS-measurements confirm a role of TbPH1 in cell cycle progression and hint at an error in the time window after kDNA replication but before mitosis. Nuclear mitosis seems to be delayed but not inhibited. This finding would further need to be supported by DAPI-countings. TbPH1 is localized throughout the cytosol, accumulating in a spot-like pattern in both procyclic and long slender bloodstream form *T. brucei*. When extracting the cytoskeleton, it was revealed that the protein is especially present in between the nucleus and the kinetoplast (see Figure 19) as well as along what may be FAZ. Co-localizations of TbPH1-V5 with diverse organellar markers did not show any complete overlap of signals, although some partial co-localization was seen with acidocalcisomes, and to a lesser degree with mitochondria, endoplasmic reticulum and FAZ. Further investigation of localization by means of biochemical fractionations showed that the protein is not freely dispersed throughout the cytosol but is in either some compartment or could be tightly associated with another structure such as microtubules. The NP40-fractionation

result supports the findings of the digitonin-fractionation as it also points at a localization of TbPH1 in either some kind of granule or organelle or that it is very tightly associated with microtubules. The immunoprecipitation and mass spectrometry data then revealed that TbPH1 interacts with at least one other protein – TbKIF11.

5. OUTLOOK

There is a lot still to be investigated about the protein TbPH1. Besides the already mentioned verifications and experiments to be repeated, there is a great variety of experiments that are interesting to conduct:

Differential staining of nucleus and kinetoplast [119] with a combination of either FACS-measurements or taking fluorescence-microscopy pictures for automated image analysis of the micrographs is a possibility to get a more precise measurement of the impact of the TbPH1-RNAi on the cell cycle. The FACS-measurement would provide a better distinction in between 1N1K and 1N2K cells and the automated image analysis of micrographs would provide a better statistical strength as more cells could be counted in comparison with simple DAPI-counts, which have to be done manually.

To see whether silencing TbPH1 affects organelle inheritance, immunofluorescence assays with organellar markers could be conducted on RNAi-induced cells. Immunogold-labeling and transmission electron microscopy would give further hints of where the protein is located exactly in the cell.

Mutational studies of the in trypanosomatids conserved methyl-arginine and the phospho-serine site for instance would give an idea about the necessity of those post-translational modifications.

To see if the homeodomain-like motif of TbPH1 is binding nucleic acids, cross-linking with UV-light and subsequent immunoprecipitation with radiolabeling of co-immunprecipitated RNA or DNA can be done.

In addition to all the experiments for TbPH1, the role of its interaction partner, TbKIF11 will be further investigated as well: tagging of TbKIF11 in the TbPH1-V5 cell line and immunofluorescence assays will show if the two proteins are truly co-localizing. Immunoprecipitation of TbKIF11 can confirm the observed interaction of the two proteins. Knocking down TbKIF11 and subsequently doing the same cell cycle studies as with TbPH1 will reveal if it exhibits the same defects in the cell cycle. If this is the case, then TbPH1 is more likely to be a regulating factor of TbKIF11.

6. CITATIONS

[1] Jannin J, Cattand P (2004) Treatment and control of human African trypanosomiasis. *Curr Opin Infect Dis* **17:**565–571.

[2] Bringaud, F., Rivière,L, Coustou, V. (2006) Energy metabolism of trypanosomatids: adaption to available carbon sources. *Mol Biochem Parasitol*, **149(1)**:1-9.

[3] Vickerman, K. (1985) Developmental cycles and biology of pathogenic trypanosomes. *Br Med Bull,* **41(2)**:105-114.

[4] Matthews, K. R. (2005) The developmental cell biology of *Trypanosoma brucei*. *J Cell Sci* **118(2)**:283-290.

[5] El-Sayed NM, Hegde P, Quackenbush J, Melville SE, Donelson J.E. (2000) The African trypanosome genome. *Int J Parasitol,* **30:**329-345.

[6] MacGregor, P., Savill, N. J., Hall, D. & Matthews, K. R. (2011) Transmission stages dominate trypanosome within-host dynamics during chronic infections. *Cell Host Microbe* **9:**310–318.

[7] Aksoy S, Gibson WC, Lehane MJ (2003) Interactions between tsetse and trypanosomes with implications for the control of trypanosomiasis. *Adv Parasitol* **53:**1–83.

[8] Vickerman K, Tetley L, Hendry KA, Turner CM (1988) Biology of African trypanosomes in the tsetse fly. *Biol Cell* **64:**109–119.

[9] D. Montagnes, E. Roberts, J. Lukeš, and C. Lowe (2012) The rise of model protozoa. *Trends Microbiol*. **20(4):**184–191.

[10] Berriman, M., Ghedin, E., Hertz-Fowler, C., Blandin, G., Renauld, H., Bartholomeu, D. C., … El-Sayed, N. M. (2005) The Genome of the African Trypanosome *Trypanosoma Brucei*. *Science*, **309(5733):** 416 LP-422.

[11] Moullan *et al*., (2015) Tetracyclines Disturb Mitochondrial Function across Eukaryotic Models: A Call for Caution in Biomedical Research. *Cell Reports* **10:**1681–1691

[12] Hashimi H, Kaltenbrunner S, Zíková A, Lukeš J (2016) Trypanosome Mitochondrial Translation and Tetracycline: No Sweat about Tet. *PLoS Pathog* **12(4):**e1005492

[13] V. Hampl, L. Hug, J. W. Leigh, J. B. Dacks, B. F. Lang, A. G. B. Simpson, and A. J. Roger (2009) Phylogenomic analyses support the monophyly of Excavata and resolve relationships among eukaryotic 'supergroups'. *Proc. Natl. Acad. Sci. U. S. A* **106(10):**3859–3864.

[14] Vickerman, K. (1962) The mechanism of cyclical development in trypanosomes of the *Trypanosoma brucei* sub-group: an hypothesis based on ultrastructural observations. *Trans R Soc Trop Med Hyg* **56:** 487–495.

[15] Anderson,W.A., and Ellis, R.A. (1965) Ultrastructure of *Trypanosoma lewisi*: flagellum, microtubules, and the kinetoplast. *J Eukaryot Microbiol* **12:**483–499.

[16] Sherwin, T., and Gull, K. (1989) The cell division cycle of *Trypanosoma brucei brucei*: timing of event markers and cytoskeletal modulations. *Philos Trans R Soc Lond B Biol Sci* **323:**573–588.

[17] Barry, J.D., and R. McCulloch (2001) Antigenic variation in trypanosomes: enhanced phenotypic variation in a eukaryotic parasite. *Adv. Parasitol.* **49:**1-70.

[18] Stebeck C.E., Pearson T.W. (1994) Major surface glycoproteins of procyclic stage African trypanosomes. *Exp Parasitol* **78:**432–436.

[19] Vickerman K. (1969) On the surface coat and flagellar adhesion in trypanosomes. *J. Cell Sci.* **5:**163–193.

[20] Woods A. (1989) Definition of individual components within the cytoskeleton of *Trypanosoma brucei* by a library of monoclonal antibodies. *J. Cell Sci*. **93:**491-500.

[21] McKean P.G. (2003) Coordination of cell cycle and cytokinesis in Trypanosoma brucei. *Current Opinion in Microbiology*, **6:**600–607

[22] Bangs, J.D. (2011). Replication of the ERES:Golgi junction in bloodstream-form African trypanosomes. *Mol Microbiol*. **82:**1433-1443.

[23] Hughes L., Borrett S., Towers K., Starborg T., and Vaughan S. (2017) Patterns of organelle ontogeny through a cell cycle revealed by whole cell reconstructions using 3D electron microscopy. *J. Cell Sci.* **130:**637-647

[24] Opperdoes F. (1977) Localization of nine glycolytic enzymes in a microbody-like organelle in *Trypanosoma Brucei*: the glycosome. *FEBS letters* **80(2):**360-364

[25] Vercesi, A.E., Moreno S.N., and Docampo R. (1994) $Ca2^{+}/H^{+}$ exchange in acidic vacuoles of *Trypanosoma brucei*. *The Biochemical journal* **304(Pt 1):**227-233.

[26] Vaughan, S. (2010) Assembly of the flagellum and its role in cell morphogenesis in *Trypanosoma brucei*. *Curr Opin Microbiol*. **13:**453-458.

[27] Woodward, R., and K. Gull (1990) Timing of nuclear and kinetoplast DNA replication and early morphological events in the cell cycle of *Trypanosoma brucei*. *Journal of cell science* **95(Pt1):**49-57.

[28] Hammarton, T.C., Monnerat, S., and Mottram, J.C. (2007) Cytokinesis in trypanosomatids. *Curr Opin Microbiol* **10:**520–527.

[29] Vickerman, K., and T.M. Preston. (1970) Spindle microtubules in the dividing nuclei of trypanosomes. *Journal of cell science* **6:**365-383.

[30] Shapiro, S. Z., Naessens, J., Liesegang, B., Moloo, S. K., Magondu, J. (1984) Analysis by flow cytometry of DNA synthesis during the life-cycle of African trypanosomes. *Acta Tropica* **41:**313-323

[31] Matthews, K.R., and Gull, K. (1994) Evidence for an interplay between cell cycle progression and the initiation of differentiation between life cycle forms of African trypanosomes. *J Cell Biol*. **125:**1147-56.

[32] Tyers, M., Haslam, R.J., Rachubinski, R.A. and Harley, C.B. (1989) Molecular analysis of pleckstrin: the major protein kinase C substrate of platelets. *J. Cell. Biochem*. **40:**133–145.

[33] Saraste M, Hyvonen M. (1995) Pleckstrin homology domains: a fact file. *Curr. Opin. Struct. Biol.* **5:**403–8

[34] Chothia C, Lesk AM. (1986) The relationship between divergence of sequence and structure in proteins*. EMBO J*. **5:**823–26

[35] Scheffzek K., Welti S. (2012) Pleckstrin homology (PH) like domains – versatile modules in protein–protein interaction platforms, *FEBS Letters* **586:**2662–2673

[36] Macias, M.J., Musacchio, A., Ponstingl, H., Nilges, M., Saraste, M. and Oschkinat, H. (1994) Structure of the pleckstrin homology domain from b-spectrin. *Nature* **369:**675–677.

[37] Yoon, H.S., Hajduk, P.J., Petros, A.M., Olejniczak, E.T., Meadows, R.P. and Fesik, S.W. (1994) Solution structure of a pleckstrin-homology domain. *Nature* **369:**672–675.

[38] Lemmon, M.A. and Ferguson, K.M. (2000) Signal-dependent membrane targeting by pleckstrin homology (PH) domains. *Biochem. J.* **350(Pt 1):**1–18.

[39] Ingley, E. and Hemmings, B.A. (1994) Pleckstrin homology (PH) domains in signal transduction. *J. Cell. Biochem.* **56:**436–443.

[40] Musacchio, A., Gibson, T., Rice, P., Thompson, J. and Saraste, M. (1993) The PH domain: a common piece in the structural patchwork of signalling proteins. *Trends Biochem. Sci.* **18:**343–348.

[41] Gibson, T.J., Hyvonen, M., Musacchio, A., Saraste, M. and Birney, E. (1994) PH domain: the first anniversary. *Trends Biochem. Sci.* **19:**349–353.

[42] Yang, J.T., R.A. Laymon, and L.S. Goldstein (1989) A three-domain structure of kinesin heavy chain revealed by DNA sequence and microtubule binding analysis. *Cell* **56:**879-889

[43] Kull, F. J., Sablin, E. P., Lau, R., Fletterick, R. J. and Vale, R. D. (1996) Crystal structure of the kinesin motor domain reveals a structural similarity to myosin. *Nature* **380:**550-555.

[44] Sablin, E. P., Kull, F. J., Cooke, R., Vale, R. D. and Fletterick, R. J. (1996). Crystal structure of the motor domain of the kinesin-related motor ncd. *Nature* **380:**555- 559.

[45] Kim, A. J. and Endow, S. A. (2000). A kinesin family tree. *J. Cell Sci.* **113:**3681-3682.

[46] Rice, S., Lin, A. W., Safer, D., Hart, C. L., Naber, N., Carragher, B. O., Cain, S. M., Pechatnikova, E., Wilson-Kubalek, E. M., Whittaker, M. et al. (1999) A structural change in the kinesin motor protein that drives motility. *Nature* **402:**778-784.

[47] Yun, M., Zhang, X., Park, C.-G., Park, H.-W. and Endow, S. A. (2001) A structural pathway for activation of the kinesin motor ATPase. *EMBO J.* **20:**2611-2618.

[48] Hirose, K., Akimaru, E., Akiba, T., Endow, S. A. and Amos, L. A. (2006) Large conformational changes in a kinesin motor catalysed by interaction with microtubules. *Mol. Cell* **23:**913-923.

[49] Endow, S. A. (1999) Determinants of molecular motor directionality. *Nat. Cell Biol.* **1:**163-167.

[50] Howard, J., Hudspeth, A. J. and Vale, R. D. (1989) Movement of microtubules by single kinesin molecules. *Nature* **342:**154-158.

[51] Block, S. M., Goldstein, L. S. B. and Schnapp, B. J. (1990) Bead movement by single kinesin molecules studied with optical tweezers. *Nature* **348:**348-352.

[52] Hackney, D. D. (1995) Highly processive microtubulestimulated ATP hydrolysis by dimeric kinesin head domains. *Nature* **377:**448-450.

[53] Endow, S. A. and Higuchi, H. (2000) A mutant of the motor protein kinesin that moves in both directions on microtubules. *Nature* **406:**913-916.

[54] deCastro, M. J., Fondecave, R. M., Clarke, L. A., Schmidt, C. F. and Stewart, R. J. (2000) Working strokes by single molecules of the kinesin-related microtubule motor ncd. *Nat. Cell Biol.* **2:**724-729.

[55] Endow, S. A. and Komma, D. J. (1997) Spindle dynamics during meiosis in Drosophila oocytes. *J. Cell Biol.* **137:**1321-1336.

[56] Goshima, G., Wollman, R., Stuurman, N., Scholey, J. M. and Vale, R. D. (2005) Length control of the metaphase spindle. *Curr. Biol.* **15:**1979-1988.

[57] Rogers, G. C., Rogers, S. L., Schwimmer, T. A., Ems-McClung, S. C., Walczak, C. E., Vale, R. D., Scholey, J.M. and Sharp, D. J. (2004) Two mitotic kinesins cooperate to drive sister chromatid separation during anaphase. *Nature* **427:**364-370

[58] Tao, L., Mogilner, A., Civelekoglu-Scholey, G., Wollman, R., Evans, J., Stahlberg, H. and Scholey, J. (2006) A homotetrameric Kinesin-5, KLP61F, bundles microtubules and antagonizes Ncd in motility assays. *Curr. Biol.* **16:**2293-2302.

[59] Manning, B. D., Barrett, J. G., Wallace, J. A., Granok, H. and Snyder, M. (1999) Differential regulation of the Kar3p kinesin-related protein by two associated proteins, Cik1p and Vik1p. *J. Cell Biol.* **144:**1219-1233.

[60] Barrett, J. G., Manning, B. D. and Snyder, M. (2000) The Kar3p kinesin-related protein forms a novel heterodimeric structure with its associated protein Cik1p. *Mol. Biol. Cell* **11:**2373-2385.

[61] Chu, H. M. A., Yun, M., Anderson, D. E., Sage, H., Park, H.-W. and Endow, S. A. (2005). Kar3 interaction with Cik1 alters motor structure and function. *EMBO J.* **24:**3214-3223.

[62] Scott M.P., Weiner A.J. (1984) Structural relationships among genes that control development: sequence homology between the Antennapedia, Ultrabithorax, and fushi tarazu loci of Drosophila. *Proc Natl Acad Sci U S A.* **81(13):**4115-9.

[63] McGinnis W., Levine M.S., Hafen E., Kuroiwa A., Gehring W.J. (1984) A conserved DNA sequence in homoeotic genes of the Drosophila Antennapedia and bithorax complexes. *Nature.* **308(5958):**428-33.

[64] Dekker N., Cox,M., Boelens,R., Verrijzer,C., van der Vliet,P. and Kaptein,R. (1993) Solution structure of the POU-specific DNA-binding domain of Oct-1. *Nature* **362:**852–855.

[65] Endo T., Ohta,K., Saito,T., Haraguchi,K., Nakazato,M., Kogai,T. and Onaya,T. (1994) Biochem. Biophys. Res. Commun., **204:**31358–31363.

[66] Gruschus J., Tsao,D., Wang,L., Nirenberg,M. and Ferretti,J. (1997) Interactions of the vnd/NK-2 homeodomain with DNA by nuclear magnetic resonance spectroscopy: basis of binding specificity. *Biochemistry*, **36:**5372–5380.

[67] Kissinger C., Liu,B., Martin-Blanco,E., Kornberg,T. and Pabo,C. (1990) Crystal structure of an engrailed homeodomain-DNA complex at 2.8 Å resolution: A framework for understanding homeodomain-DNA interactions. *Cell*, **63:**579–590.

[68] Ceska T., Lamers,M., Monaci,P., Nicosia,A., Cortese,R. and Suck,D. (1993) The x-ray structure of an atypical homeodomain present in the rat liver transcription factor LFB1/HNF1 and implications for DNA binding. *EMBO J.,* **12(5):** 1805–1810.

[69] Liu B., Kissinger,C. and Pabo,C. (1990) Crystallization and preliminary X-ray diffraction studies of the engrailed homeodomain and of an engrailed homeodomain/DNA complex. *Biochem. Biophys. Res. Commun.*, **171:**257–259.

[70] Qian Y., Billeter,M., Otting,G., Muller,M., Gehring,W. and Wuthrich,K. (1989) *Cell*, **59:**573–580.

[71] Qian Y., Furukubo-Tokunaga,K., Resendez-Perez,D., Muller,M., Gehring,W. and Wuthrich,K. (1994) *J. Mol. Biol*. **238:**333–345.

[72] Wolberger C., Vershon,A., Liu,B., Johnson,A. and Pabo,C. (1991) *Cell*, **67:**517–528.

[73] Dubnau J., Struhl G. (1997) RNA recognition and translational regulation by a homeodomain protein. *Nature* 14; **388(6643):**697.

[74] Wolberger C. (1996) Homeodomain interactions. *Curr Opin Struct Biol*. **6:**62–68.

[75] Wickstead B, Gull K. (2006) A "holistic" kinesin phylogeny reveals new kinesin families and predicts protein functions. *Mol Biol Cell*; **17:**1734–43.

[76] Desai, A. et al. (1999) Kin I kinesins are microtubule-destabilizing enzymes. *Cell;* **96:**69–78

[77] Moores, C.A. et al. (2002) A mechanism for microtubule depolymerization by KinI kinesins. *Mol. Cell*; **9:**903–909

[78] Noda, Y. et al. (1995) KIF2 is a new microtubule-based anterograde motor that transports membranous organelles distinct from those carried by kinesin heavy chain or KIF3A/B. *J. Cell Biol*. **129:**157–167

[79] Chan, K.Y., Ersfeld, K. (2010) The role of the Kinesin-13 family protein TbKif13-2 in flagellar length control of *Trypanosoma brucei*. *Molecular and Biochemical Parasitology;* **174:**137-140

[80] Chan KY, Matthews KR, Ersfeld K (2010) Functional Characterisation and Drug Target Validation of a Mitotic Kinesin-13 in *Trypanosoma brucei. PLoS Pathog* **6(8):** e1001050. doi:10.1371/journal.ppat.1001050

[81] JJ Vincente, L. Wordeman, (2015) Mitosis, microtubule dynamics and the evolution of kinesins. *Experimental Cell Research* **334:**61-69

[82] Nislow, C. et al. (1992) A plus-end-directed motor enzyme that moves antiparallel microtubules in vitro localizes to the interzone of mitotic spindles. *Nature* **359:**543–547

[83] Adams, R.R. et al. (1998) Pavarotti encodes a kinesin-like protein required to organize the central spindle and contractile ring for cytokinesis. *Genes Dev.* **12:**1483–1494

[84] Hill, E. et al. (2000) The Rab6-binding kinesin, Rab6-KIFL, is required for cytokinesis. *EMBO J.* **19:**5711–5719

[85] Lillie, S.H. and Brown, S.S. (1994) Immunofluorescence localization of the unconventional myosin, Myo2p, and the putative kinesinrelated protein, Smy1p, to the same regions of polarized growth in *Saccharomyces cerevisiae*. *J. Cell Biol.* **125:**825–842

[86] Wolf, F.W. et al. (1998) Vab-8 is a key regulator of posteriorly directed migrations in C. elegans and encodes a novel protein with kinesin motor similarity. *Neuron* **20:**655–666

[87] Lillie, S.H. and Brown, S.S. (1998) Smy1p, a kinesin-related protein that does not require microtubules. *J. Cell Biol.* **140:**873–883

[88] Cole, D.G. et al. (1994) A "slow" homotetrameric kinesin-related motor protein purified from Drosophila embryos. *J. Biol. Chem.* **269:**22913–22916

[89] Enos, A.P. and Morris, N.R. (1990) Mutation of a gene that encodes a kinesin-like protein blocks nuclear division in A. nidulans. *Cell* **60:**1019–1027

[90] Wickstead B, Ersfeld K, Gull K (2002) Targeting of a tetracycline-inducible expression system to the transcriptionally silent minichromosomes of *Trypanosoma brucei*. *Mol Biochem Parasitol* **125:**211–216

[91] Li, Y., Li, Z., and Wang, C.C. (2003) Differentiation of *Trypanosoma brucei* may be stage non-specific and does not require progression of cell cycle. *Mol Microbiol;* **49:**251–265.

[92] Li, H., Hu. H., and Li, Z. (2012) A kinetoplastid-specific kinesin is required for cytokinesis and for maintenance of cell morphology in *Trypnaosoma brucei. Mol Microbiol;* **83(3):**565-578.

[93] H. Hu, Yu Z., Chasse A.E., Chu F., and Li Z. (2012) An orphan kinesin in trypanosomes cooperates with a kinetoplastid-specific kinesin to maintain cell morphology by regulating subpellicular microtubules. *J Cell Sci*; **125:**4126-4136

[94] R. Brun and Schönenberger (1979) Cultivation and in vitro cloning or procyclic culture forms of *Trypanosoma brucei* in a semi-defined medium. *Short communication. Acta Trop.* **36:**289–292

[95] S. K. Poon, L. Peacock, W. Gibson, K. Gull, and S. Kelly (2012) A modular and optimized single marker system for generating *Trypanosoma brucei* cell lines expressing T7 RNA polymerase and the tetracycline repressor. *Open Biol*. **2(2):**110037

[96] E. Wirtz, S. Leal, C. Ochatt, and G. a Cross (1999) A tightly regulated inducible expression system for conditional gene knock-outs and dominant-negative genetics in *Trypanosoma brucei*. *Mol. Biochem. Parasitol*., **99(1):**89–101,

[97] Alsford, S., Kawahara, T., Glover, L. & Horn, D. (2005) Tagging a *T. brucei* rRNA locus improves stable transfection efficiency and circumvents inducible expression position effects. *Molecular and biochemical parasitology* **144:**142-148

[98] S. Dean, J. Sunter, R. J. Wheeler, I. Hodkinson, E. Gluenz, K. Gull, and S. Dean (2015) A toolkit enabling efficient, scalable and reproducible gene tagging in trypanosomatids," *Open Biol.*, **5:**140197

[99] Hashimi H., Zíková A., Panigrahi A.K., Stuart K.D., Lukeš J. (2008) TbRGG1, an essential protein involved in kinetoplastid RNA metabolism that is associated with a novel multiprotein complex. *RNA* **14:**970–980

[100] Morriswood, B., Havlicek, K., Demmel, L., Yavuz, S., Sealey-Cardona, M., Vidilaseris, K., Warren, G. (2013). Novel Bilobe Components in Trypanosoma brucei Identified Using Proximity-Dependent Biotinylation. *Eukaryotic Cell*, **12(2):**356–367

[101] Basu S., Leonard J.C., Desai N., Mavridou D.A.I., Tang K.H., Goddard A.D., Ginger M.L., Lukeš J., Allen J.W.A. (2013) Divergence of Erv1-Associated Mitochondrial Import and Export Pathways in Trypanosomes and Anaerobic Protists. *Eukaryot Cell.* **12(2):**343–355.

[102] Fritz, M., Vanselow, J., Sauer, N., Lamer, S., Goos, C., Siegel, T. N., … Kramer, S. (2015). Novel insights into RNP granules by employing the trypanosome's microtubule skeleton as a molecular sieve. *Nucleic Acids Research*, ***43*(16):**8013–8032.

[103] U. K. Laemmli, (1970) Cleavage of structural proteins during the assembly of the head of bacteriophage T4. *Nature*, **227(5259):**680–685

[104] Aslett M., Aurrecoechea C., Berriman M. *et al* (2010) TriTrypDB: a functional genomic resource for the Trypanosomatidae. *Nucleic Acids Res.* **38(suppl_1):**D457-D462.

[105] Alva V., Nam S.Z., Söding J., Lupas A.N. (2016) The MPI bioinformatics Toolkit as an integrative platform for advanced protein sequence and structure analysis. *Nucleic Acids Res*. pii: gkw348.

[106] Urbaniak, M. D., Martin, D. M. A., & Ferguson, M. A. J. (2013). Global Quantitative SILAC Phosphoproteomics Reveals Differential Phosphorylation Is Widespread between the Procyclic and Bloodstream Form Lifecycle Stages of *Trypanosoma brucei*. *Journal of Proteome Research*, **12(5):**2233–2244.

[107] Lott, K., Li, J., Fisk, J. C., Wang, H., Aletta, J. M., Qu, J., & Read, L. K. (2013). Global Proteomic Analysis in Trypanosomes Reveals Unique Proteins and Conserved Cellular Processes Impacted by Arginine Methylation. *Journal of Proteomics*, ***91*:**210–225.

[108] 12. Dubnau J., Struhl G. (1997), RNA recognition and translational regulation by a homeodomain protein. *Nature* **14:**388(6643):697.

[109] Emmer B.T., Nakayasu E.S., Souther C., Choi H., Sobreira T.J., Epting C.L., Nesvizhskii A.I., Almeida I.C., Engman D.M. (2011) Global analysis of protein palmitoylation in African trypanosomes. *Eukaryot Cell*. **10(3):**455-463.

[110] Linder M.E., Deschenes R.J., (2007) Palmitoylation: policing protein stability and traffic. Nature **8:**74-84

[111] Pradel L.C., Bonhivers M., Landrein N., Robinson D.R. (2006) NIMA-related kinase TbNRKC is involved in basal body separation in *Trypanosoma brucei*. *J Cell Sci.* **119:**1852–1863.

[112] Hammarton T.C., Kramer S. (2007), *Trypanosoma brucei* polo-like kinase is essential for basal body duplication, kDNA segregation and cytokinesis. *Mol. Microbiol.* **65(5):** 1229-1248

[113] Sharma, N., Kosan, Z. A., Stallworth, J. E., Berbari, N. F., & Yoder, B. K. (2011). Soluble levels of cytosolic tubulin regulate ciliary length control. *Molecular Biology of the Cell*, ***22*(6):**806–816.

[114] Walker, J. E., Saraste, M., Runswick, M. J., & Gay, N. J. (1982). Distantly related sequences in the alpha- and beta-subunits of ATP synthase, myosin, kinases and other ATP-requiring enzymes and a common nucleotide binding fold. *The EMBO Journal*, **1(8):**945–951.

[115] Hanson P.I., Whiteheart S.W. (2005). AAA+ proteins: have engine, will work. *Nat. Rev. Mol. Cell Biol.* ***6(7):****519–29*

[116] Bell, C.E. (2005) Structure and mechanism of *Escherichia coli* RecA ATPase. *Mol. Microbiol*. **58(2):**358-366

[117] Konola J.K., Logan K.M., Knight K.L., (2004) Novel and deviant Walker A ATP-binding motifs in bacteriophage large terminase–DNA packaging proteins. *Virology* **321:**217– 221

[118] Dean S., Sunter J.D., Wheeler R.J, (2016) TrypTag.org: A Trypanosome Genome-wide Protein Localization Resource, *Trends in Parasitology* **33(2):**80-82

[119] Wheeler R.J, Gull K., Gluenz E., (2012) Detailed interrogation of trypanosome cell biology via differential organelle staining and automated image analysis. *BMC Biology* **10:1**

[120] Schultz et al (1998) SMART, a simplemodular architecture research tool: Identification of signaling domains. *Proc. Natl. Acad. Sci. USA* 95:5857-5864

[121] Letunic, I., Doerks, T., & Bork, P. (2015) SMART: recent updates, new developments and status in 2015. *Nucleic Acids Research*, **43**(Database issue): D257–D260

[122] Alsford, S., Turner, D. J., Obado, S. O., Sanchez-Flores, A., Glover, L., Berriman, M., … Horn, D. (2011). High-throughput phenotyping using parallel sequencing of RNA interference targets in the African trypanosome. *Genome Research*, **21(6):**9

7. APPENDIX

Overview:

A study from Moullan et al. [11] demonstrated that tetracycline has an unintended effect on mitochondrial translation in animals and plants. As tetracyclines are widely used in agriculture and biomedical research, the study was raising concerns about the usability of the antibiotic in the research of those eukaryotic model systems. In this PLOS Pathogen Pearl, we were able to show that *T. brucei* is not affected in this way by tetracyclines due to its highly divergent mitochondrial ribosome.

Citation:

Hashimi H., Kaltenbrunner S., Zíková A., Lukeš J. (2016) Trypanosome Mitochondrial Translation and Tetracycline: No Sweat about Tet. *PLoS Pathog.* **12(4):**e1005492

PLOS | PATHOGENS

PEARLS

Trypanosome Mitochondrial Translation and Tetracycline: No Sweat about Tet

Hassan Hashimi[1,2]*, Sabine Kaltenbrunner[2], Alena Zíková[1,2], Julius Lukeš[1,2,3]

1 Institute of Parasitology, Biology Centre, Czech Academy of Sciences, University of South Bohemia, Czech Republic, **2** Faculty of Science, University of South Bohemia, Czech Republic, **3** Canadian Institute for Advanced Research, Toronto, Canada

* hassan@paru.cas.cz

Overview

A recent study vividly demonstrates the unintended impact of the antibiotic tetracycline (Tet) on animal and plant mitochondrial translation, which corresponds to the α-proteobacterial origin of the organelle. This effect was ultimately manifested by an impact on the cellular, and even organismal, levels in the studied eukaryotes. Thus, widespread use of Tet in agriculture and biomedical research is now under scrutiny. Interestingly, Tet does not affect this process in trypanosomatids. The highly divergent nature of trypanosomatid mitochondrial ribosomes may explain why these flagellates are insensitive to Tet.

Citation: Hashimi H, Kaltenbrunner S, Zíková A, Lukeš J (2016) Trypanosome Mitochondrial Translation and Tetracycline: No Sweat about Tet. PLoS Pathog 12(4): e1005492. doi:10.1371/journal.ppat.1005492

Editor: Laura J Knoll, University of Wisconsin Medical School, UNITED STATES

Published: April 21, 2016

Funding: This work was funded by Grant Agency of the Czech Republic (grant number: 15-21974S), ERC CZ (grant number: LL1205). The funders had no role in study design, data collection and analysis, decision to publish, or preparation of the manuscript.

Competing Interests: The authors have declared that no competing interests exist.

How Does Tetracycline Affect Mitochondria?

A study recently published by Moullan and coauthors [1] pronounced that even low doses in the μg/ml range of tetracycline (Tet) have an adverse effect on mitochondrial function in several model eukaryotes, ranging from metazoa to plants to in vitro human cultures. This paper brought into the limelight the danger of profuse usage of this class of antibiotics not only prophylactically, e.g., to maintain and promote growth in livestock, but also in biomedical research. The emergence of elegant platforms for Tet-controlled transcription by Tet-On and Tet-Off systems for inducing and suppressing gene expression, respectively, in a variety of eukaryotic models underlies the widespread use of this antibiotic in experimental biology. Importantly, as illustrated by these authors, even low, single-digit μg/ml concentrations of Tet also induced what has been termed "mitonuclear protein imbalance," in which the proportion of nucleus-encoded proteins imported into the organelle versus those arising from mitochondrial genes increases [1]. This subtle but perceptible phenotype, long overlooked, consequently impairs mitochondrial functions, such as respiration, and also induces significant detrimental changes at the organismal level, such as diminished growth and delayed development. Interestingly, a beneficial impact was observed in *Caenorhabditis elegans*, in which treatment with the Tet-class antibiotic doxycycline (Dox) mitigated the age-related decline in motility. Thus, the authors concluded that the vast amount of data produced using Tet-controlled gene expression may be confounded by the unintended disruption of the given model's mitochondria. They also cautioned against the future use of Tet-On and Tet-Off systems [1].

How Does Tetracycline Inhibit Mitochondrial Translation?

The mitonuclear protein imbalance caused by the antibiotic in question arises from its long-ago established inhibition of mitochondrial translation [2], which coheres to the α-proteobacterial origin of the organelle. More specifically, Tet prevents the accommodation of aminoacylated

(aa-) tRNA into its entry point to the mitochondrial ribosome, the A-site [3,4]. Two solved structures of the bacterium *Thermus thermophilis* 30S ribosomal small subunit (SSU) bound by Tet share two sites where the antibiotic attaches to facilitate its inhibitory action [5,6]. In the first location adjacent to the A-site, the compound intercalates into a pocket formed by the double-stranded (ds) helices H31 and H34 of 16S ribosomal (r) RNA, the polyribonucleotide component of the SSU, and binds to the sugar-phosphate backbone of H34. Within this position, Tet sterically hinders aa-tRNA attachment into the A-site of the ribosome, thus inhibiting translation [3,5,6]. A second Tet-binding position identified in both structures involves another ds 16S rRNA helix designated H27, a switch region that plays a role in selection of the proper aa-tRNA at the A-site [7]. Although this would not directly hinder aa-tRNA accommodation into the ribosome, it may still contribute to the disruption of this translational step [3]. These secondary structural motifs of the bacterial SSU 16S rRNA that interact with Tet are conserved in the homologous SSU rRNA of plant and animal mitochondrial ribosomes (Fig 1) [8,9]. Thus, the inhibitory effect of Tet on mitochondrial translation leading to the consequences described by Moullan and coauthors [1] could rely on a very similar mechanism as described for bacterial ribosomes [3,5,6].

How Does Tetracycline Affect Trypanosomes?

What does all this mean for the large community of molecular parasitologists studying *Trypanosoma brucei*? The development of Tet-controlled transcription for functional analysis of nuclear genes, mostly via straightforward application of RNA interference and the expression of exogenous genes, represented a major breakthrough for the field [10]. This platform has been so successful in *T. brucei* that it has also been implemented to study various *Leishmania* species [11]. However, are all these data, acquired over two decades, confounded by the recently reported Tet-triggered mitonuclear protein imbalance plaguing typical model systems of biomedical research [1]? Should the future application of this useful platform be reconsidered? Reassuringly, the answer to both questions is no. As seen in Fig 2, Dox exhibits a very high EC_{50} value of about 620 μg/ml in cultured procyclic *T. brucei*, the life cycle stage residing in the tsetse fly midgut that bears an actively respiring mitochondrion [12]. Indeed, up to 50 μg/ml of Dox does not negatively impact parasite fitness. This observation recapitulates tacit knowledge in the field that Tet treatment at the standard induction dose of 1 μg/ml, considerably lower than the aforementioned concentration, does not hamper *T. brucei* cell division. In contrast, when mitochondrial gene expression is down-regulated, ultimately decreasing the levels of the organellar gene products that are generated by mitochondrial ribosomes, an obvious growth-inhibition phenotype is observed (e.g., [13] and [14]).

Is Trypanosome Mitochondrial Translation Affected by Tetracycline?

The seeming insensitivity of trypanosomatids to Tet treatment occurs because mitochondrial translation is not susceptible to the antibiotic. Studies done on procyclic *T. brucei* and the related species *Leishmania tarentolae* have demonstrated that their mitochondrial translation is not affected even when they are grown in the presence of 100 μg/ml Tet [13,15], a concentration greatly exceeding those used by Moullan and coauthors [1], but half that of the maximal concentration not affecting procyclic *T. brucei* fitness (Fig 2).

Could one of the mechanisms of bacterial Tet resistance, Tet efflux, Tet degradation, rRNA mutations, or the participation of ribosomal protection proteins (RPPs) [3,4] underlie the Tet resistance of trypanosomatid mitochondrial translation? Most RPPs are homologous to prokaryotic elongation factors EF-Tu and EF-G, a structural feature that allows these proteins to

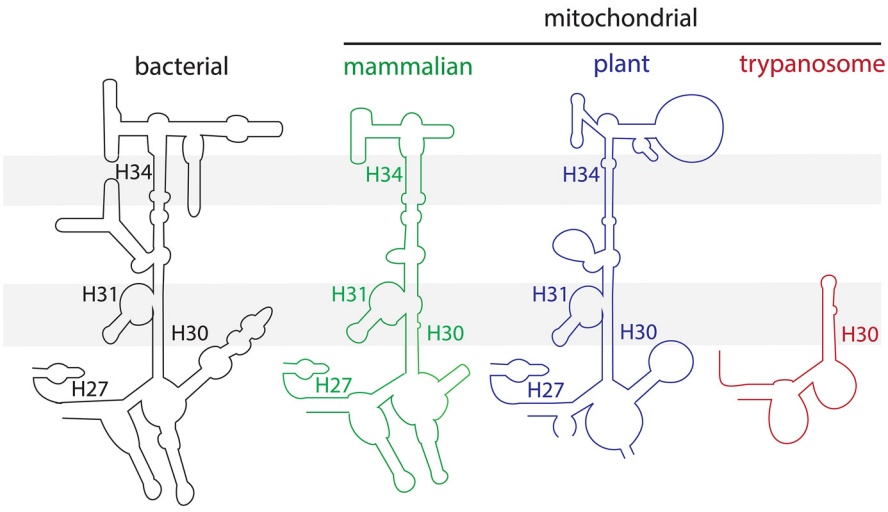

Fig 1. The ribosomal small subunit rRNA loops containing H31 and H34, as well as H27, double-stranded helices from bacteria (black) plus the mitochondria of mammals (green), plants (blue) and trypanosomes (red). Grey shading highlights the location of H31 and H34 in the SSU rRNAs bearing these motifs, as well as their absence in the same region of the trypanosomatid SSU rRNA. Helix H30, which is conserved throughout all the depicted rRNAs, is also indicated as a reference point. Adapted from [8] and [9].

doi:10.1371/journal.ppat.1005492.g001

access and dislodge Tet from the ribosome A-site [3,4]. However, only genes encoding mitochondrial EF-Tu, EF-G1, and EF-G2 have been identified in trypanosomatid genomes [14], implying the lack of RPPs to perform the same function on trypanosomatid mitochondrial ribosomes. With the current state of knowledge, it is still not possible to rule out Tet efflux of the mitochondrion or Tet degradation within the organelle with confidence. However, available data allow exploring the last possibility that key differences in the SSU rRNA sequence may underlie the Tet insensitivity of trypanosomatid mitochondrial translation.

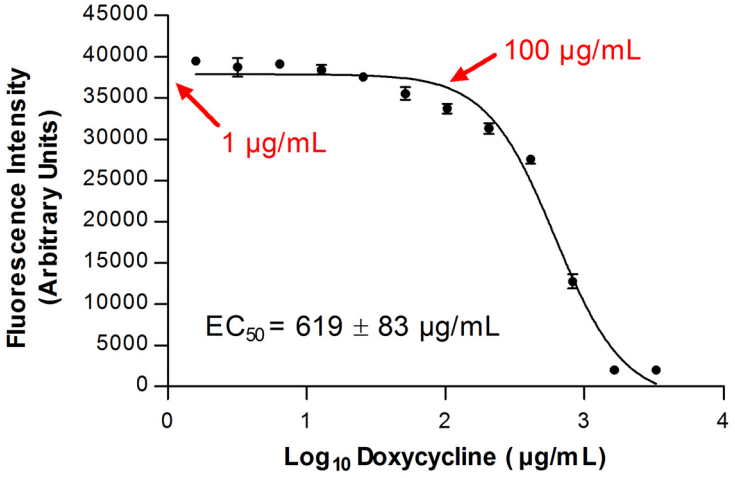

Fig 2. Effect of 24 hour doxycycline exposure on the viability of procyclic stage *T. brucei*. Data points represent the mean cell viability ± standard error of the mean (SEM) ($n = 4$), as measured by the Alamar Blue fluorescent dye assay. *X*-axis, µg/ml doxycycline (log scale); *y*-axis Alamar Blue fluorescence intensity in arbitrary units; doxycycline EC_{50} value calculated from curve given on lower left. Red arrows indicate points corresponding to 1 and 100 µg/ml concentrations on the *x*-axis. The assay was performed as previously described [19].

doi:10.1371/journal.ppat.1005492.g002

Are Unique Features of Trypanosome Mitochondrial Ribosomes Responsible for the Insensitivity of Mitochondrial Translation to Tetracycline?

The mitochondrial ribosomes of both *T. brucei* and *L. tarentolae* are quite different from their counterparts in animals, plants, and bacteria. The 9S SSU and 12S large subunit (LSU) rRNAs are considerably reduced as compared to the rRNAs of aforementioned organisms, representing the smallest known orthologs of these molecules [9,16]. To compensate for this deficiency in the rRNA component of the ribosome, trypanosomatids have experienced an expansion in the number of mitochondrial ribosomal proteins, most of which are unique to these kinetoplastid flagellates. The solved structure of the *L. tarentolae* mitochondrial ribosome [9] further refines this information in terms of the lack of Tet-sensitivity of the ribosome. Here, we see that the loop of the 9S rRNA, which encompasses the important Tet-binding H31 and H34 helices present in other SSU rRNAs, is significantly truncated (Fig 1). This loop, which also contains rRNA elements normally needed for aa-tRNA accommodation into the A-site, is replaced in mitochondrial ribosomes by trypanosomatid-specific proteins [9]. In this milieu, the Tet-binding site is ablated by the lack of the H31 and H34 helices, the latter of which ordinarily provides the sugar-phosphate backbone for attachment of the antibiotic [3,5,6]. Furthermore, the H27 helix that represents another Tet-binding site is considerably reduced in trypanosomatid 9S rRNA.

The observation that the contact points for Tet-binding are lacking in the trypanosomatid mitochondrial SSU is not proof that these structural features are completely responsible for organellar translation's insensitivity to treatment with this antibiotic. However, their conspicuous absence represents the most parsimonious hypothesis for this phenomenon considering the current state of knowledge. If this hypothesis is true, trypanosomatid mitochondrial ribosomes may be informative in comparative studies further investigating the mechanism of Tet inhibition of translation in other bacterial and organellar systems. Certainly, the insensitivity of trypanosomatid mitochondrial translation to Tet represents yet another exquisite example of the extreme evolutionary divergence of this group of protists, considering this trait is found in the bacterial domain of life, which gave rise to mitochondria, and remains conserved in the widely separated plant and mammalian eukaryotic clades. This phenomenon also belongs to a long line of discoveries made in trypanosomatids that have contributed to our understanding of biological processes vital to eukaryotes as a whole, epitomized by renowned examples, including the linkage of glycoproteins to the plasma membrane via glycosylphosphatidylinositol anchors [17] and the shaping of transcriptomes by RNA editing [18]. It is also reassuring to know that as we unravel more about the fascinating biology of trypanosomatids, our genetic tools are precise.

References

1. Moullan N, Mouchiroud L, Wang X, Ryu D, Williams EG, et al. (2015) Tetracyclines disturb mitochondrial function across eukaryotic models: A call for caution in biomedical research. Cell Reports 10: 1681–1691.
2. Clark-Walker GD, Linnane AW (1966) In vivo differentiation of yeast cytoplasmic and mitochondrial protein synthesis with antibiotics. Biochemical and Biophysical Research Communications 25: 8–13. PMID: 5971759
3. Connell SR, Tracz DM, Nierhaus KH, Taylor DE (2003) Ribosomal protection proteins and their mechanism of tetracycline resistance. Antimicrobial Agents and Chemotherapy 47: 3675–3681. PMID: 14638464
4. Chopra I, Roberts M (2001) Tetracycline antibiotics: mode of action, applications, molecular biology, and epidemiology of bacterial resistance. Microbiology and Molecular Biology Reviews 65: 232–260. PMID: 11381101

5. Pioletti M, Schlunzen F, Harms J, Zarivach R, Gluhmann M, et al. (2001) Crystal structures of complexes of the small ribosomal subunit with tetracycline, edeine and IF3. The EMBO Journal 20: 1829–1839. PMID: 11296217
6. Brodersen DE, Clemons WM Jr., Carter AP, Morgan-Warren RJ, Wimberly BT, et al. (2000) The structural basis for the action of the antibiotics tetracycline, pactamycin, and hygromycin B on the 30S ribosomal subunit. Cell 103: 1143–1154. PMID: 11163189
7. Lodmell JS, Dahlberg AE (1997) A conformational switch in *Escherichia coli* 16S ribosomal RNA during decoding of messenger RNA. Science 277: 1262–1267. PMID: 9271564
8. Spencer DF, Schnare MN, Gray MW (1984) Pronounced structural similarities between the small subunit ribosomal RNA genes of wheat mitochondria and *Escherichia coli*. Proceedings of the National Academy of Sciences of the United States of America 81: 493–497. PMID: 6364144
9. Sharma MR, Booth TM, Simpson L, Maslov DA, Agrawal RK (2009) Structure of a mitochondrial ribosome with minimal RNA. Proceedings of the National Academy of Sciences of the United States of America 106: 9637–9642. doi: 10.1073/pnas.0901631106 PMID: 19497863
10. Matthews KR (2015) 25 years of African trypanosome research: From description to molecular dissection and new drug discovery. Molecular and Biochemical Parasitology 200: 30–40. doi: 10.1016/j.molbiopara.2015.01.006 PMID: 25736427
11. Kraeva N, Ishemgulova A, Lukeš J, Yurchenko V (2014) Tetracycline-inducible gene expression system in *Leishmania mexicana*. Molecular and Biochemical Parasitology 198: 11–13. doi: 10.1016/j.molbiopara.2014.11.002 PMID: 25461484
12. Verner Z, Basu S, Benz C, Dixit S, Dobáková E, et al. (2015) Malleable mitochondrion of *Trypanosoma brucei*. International Review of Cell and Molecular Biology 315: 73–151. doi: 10.1016/bs.ircmb.2014.11.001 PMID: 25708462
13. Nebohácová M, Maslov DA, Falick AM, Simpson L (2004) The effect of RNA interference down-regulation of RNA editing 3'-terminal uridylyl transferase (TUTase) 1 on mitochondrial de novo protein synthesis and stability of respiratory complexes in *Trypanosoma brucei*. The Journal of Biological Chemistry 279: 7819–7825. PMID: 14681226
14. Cristodero M, Mani J, Oeljeklaus S, Aeberhard L, Hashimi H, et al. (2013) Mitochondrial translation factors of *Trypanosoma brucei*: elongation factor-Tu has a unique subdomain that is essential for its function. Molecular Microbiology 90: 744–755. doi: 10.1111/mmi.12397 PMID: 24033548
15. Horváth A, Nebohácová M, Lukeš J, Maslov DA (2002) Unusual polypeptide synthesis in the kinetoplast-mitochondria from Leishmania tarentolae. Identification of individual de novo translation products. The Journal of Biological Chemistry 277: 7222–7230. PMID: 11773050
16. Zíková A, Panigrahi AK, Dalley RA, Acestor N, Anupama A, et al. (2008) *Trypanosoma brucei* mitochondrial ribosomes: affinity purification and component identification by mass spectrometry. Molecular & Cellular Proteomics 7: 1286–1296.
17. Ferguson MA (1999) The structure, biosynthesis and functions of glycosylphosphatidylinositol anchors, and the contributions of trypanosome research. Journal of Cell Science 112: 2799–2809. PMID: 10444375
18. Read LK, Lukeš J, Hashimi H (2016) Trypanosome RNA editing: the complexity of getting U in and taking U out. Wiley Interdisciplinary Reviews RNA 7: 33–51. doi: 10.1002/wrna.1313 PMID: 26522170
19. Alkhaldia AAM, Martínek J, Panicucci B, Dardonville C, Zíková A, et al. (2016) Trypanocidal action of bisphosphonium salts through a mitochondrial target in bloodstream form Trypanosoma brucei. International Journal for Parasitology: Drugs and Drug Resistance 6: 23–34.